Chapter 4

New Aspects of the Structure of D-Amino Acid Oxidase from Porcine Kidney in Solution: Molecular Dynamics Simulation and Photoinduced Electron Transfer

Arthit Nueangaudom, Kiattisak Lugsanangarm, Somsak Pianwanit, Sirirat Kokpol, Nadtanet Nunthaboot, Fumio Tanaka, Seiji Taniguchi and Haik Chosrowjan

Additional information is available at the end of the chapter

http://dx.doi.org/10.5772/intechopen.68645

Abstract

Mammalian D-amino acid oxidase (DAAO) plays an important role for D-serine metabolism in the brain and regulation of glutamatergic neurotransmission. In the present work, the structures in solution obtained by the methods of molecular dynamic simulation (MDS) and analyses of photoinduced electron transfer (ET) from aromatic amino acids to the excited isoalloxazine (Iso*) are described based upon our recent works, comparing among DAAO dimer, monomer, DAAO-benzoate (DAOB) complex dimer and monomer. The fluorescence lifetimes of DAAO and DAOB in the time domain of picoseconds and femtoseconds are used for the ET analyses as experimental data. The ET parameters (static dielectric constants near isoalloxazine (Iso), standard free energy gap (SFEG) between the photoproducts and reactants), ET rates, and related physical quantities (solvent reorganization energy, net electrostatic energy between the photoproducts and ionic groups in the proteins), in addition to MDS structures, are used to compare the protein structures. The structure of the DAOB dimer in solution obtained by MDS is substantially different from the crystal structure, and the structures of the two subunits are not equivalent in solution. The ET rates and related physical quantities also differ between the two subunits.

Keywords: D-amino acid oxidase from porcine kidney, benzoate complex, molecular dynamics simulation, dimer and monomer structures in solution, analyses of photoinduced electron transfer, rate of photoinduced electron transfer, fluorescence lifetimes

1. Introduction

D-Amino acid oxidase contains flavin adenine dinucleotide (FAD) as a cofactor and exists in a wide range of species from yeasts to humans. The enzyme catalyzes the oxidative degradation of D-amino acids to the corresponding amino acids, ammonium, and hydrogen peroxide. A number of review articles on D-amino acid oxidase (DAAO) from porcine kidney [1–3] and yeast to humans [4–6] have been reported. Mammalian D-amino acid oxidase plays an important role on D-serine metabolism in the brain and regulation of glutamatergic neurotransmission [7, 8]. Various new inhibitors of human D-amino acid oxidase have been found using in silico screening [9]. The crystal structures of DAAO are determined in the DAAO-benzoate (DAOB) complex and DAAO-*o*-aminobenzoate complex [2, 10, 11].

Photochemistry of flavins and flavoproteins [12] and the fluorescence quenching of flavins by various substances [13, 14] have been pioneered by Weber. The quenching mechanism of isoalloxazine (Iso) fluorescence upon complex formation with adenine in FAD is initially resolved by means of fluorescence lifetime measurements [15, 16], and the fluorescence quenching of Iso by indole with Iso-$(CH_2)_n$-indole diads is reported by McCormick [17]. Time-resolved fluorescence spectroscopy of flavins and flavoproteins has been reviewed by van den Berg and Visser [18]. The mechanism of the fluorescence quenching is studied in the systems of riboflavin tetrabutylate and indole, riboflavin tetrabutylate and N,N′-dimethylaniline in organic solvents [19], and flavodoxin from *Desulfovibrio vulgaris* (Miyazaki, F.) [20], by means of a picosecond transient-absorption spectroscopy. The remarkable fluorescence quenching of flavins is ascribed to fast photoinduced electron transfer (ET) from these substances to the excited Iso (Iso*). The ET mechanism in the riboflavin binding protein from egg white is also reported by means of a femtosecond transient-absorption spectroscopy [21]. A number of flavoproteins display very weak fluorescence, which decays with ultrashort lifetimes observed upon excitation with a sub-picosecond pulse laser [22–30]. These experimental results suggest that the valuable and detailed information on the microscopic structures of DAAO can be obtained through analyses of ET rates. We have developed a new method to analyze ET rates from aromatic amino acids to Iso* in flavoproteins using an electron transfer theory and MDS and the fluorescence lifetimes or decays of the flavoproteins as the experimental data [31–36].

In the present chapter, the ET analyses based upon MDS structures have been used to deduce submicroscopic features of various species of DAAO dimer, DAAO monomer, DAOB dimer, and DAOB monomer and compared them among these species.

2. Methods

2.1. Fluorescence spectroscopy of DAAO and DAOB

2.1.1. Steady-state excitation

Since fluorescence of free flavins was discovered by Weber [12–14], many workers have been working on its fluorescence characteristics. Kozioł first investigated solvent effects of the fluorescence in organic solvents [37]. However, free flavins are almost insoluble in most organic solvents, so that a number of solvents for the study were limited. Riboflavin tetrabutylate, which is soluble

in organic solvents, was synthesized by Yagi's group. Systematic study on the solvent effects of the absorption and fluorescence spectra has been working with riboflavin tetrabutylate [38]. Fluorescence of DAAO was first studied by Massey et al. [39]. McCormic et al. precisely examined on the fluorescence properties of apo- and holo-DAAO [40].

Fluorescence intensity of the bound FAD in DAAO is quite weak compared to that of free FAD, and further fluorescence polarization is also quite different between free and the bound FAD [41]. A relative fluorescence intensity of the bound FAD to free FAD is defined as $R_1 = I/I_0$, where I and I_0 are the fluorescence intensities of the enzyme solution at certain concentration and free FAD at the same concentration with the enzyme sample. A parameter R_2 is defined with experimental polarization anisotropies as $R_2 = (A - A_f) / (A_b - A)$, where A, A_f, and A_b are polarization anisotropies of an enzyme solution, free FAD, and bound FAD, respectively. Dissociation constant of FAD from DAAO (K_d) [42, 43] and relative quantum yield of the bound FAD to the free FAD (r) were obtained with Eqs. (1) and (2) [44–46]:

$$K_d = \frac{R_1}{1 + R_2 - R_1}\left\{[P]_0 - [F]_0 + \frac{R_1}{1 + R_2}[F]_0\right\} \tag{1}$$

$$r = \frac{R_1 R_2}{1 + R_2 - R_1} \tag{2}$$

In Eq. (1), $[P]_0$ and $[F]_0$ are the total concentration of the protein (apoprotein plus holoprotein) and the total concentration of FAD (free and bound FADs) in the enzyme solution.

2.1.2. Fluorescence dynamics

Time-resolved fluorescence of free flavins was first studied by means of a phase-shift method by Weber's group [15, 16]. Transient fluorescence spectroscopy of flavoproteins is most useful experimental tool for the conformational changes of flavoproteins [18]. In 1980, the fluorescence lifetimes of DAAO was first reported by means of a picosecond-resolved fluorescence spectroscopy with a mode-locked Nd:YAG laser (pulse width, 30 ps) and streak camera combination by Nakashima et al. [44, 45]. Later, the fluorescence dynamics was measured with a synchronously pumped, cavity-dumped dye laser and single-photon counting system (pulse width 35 ps) to study a temperature-induced conformational change as described later [46, 47]. The fluorescence lifetimes of DAOB, however, could not be determined in the picosecond time domain [45]. The ultrafast fluorescence dynamics of DAOB was measured in the time domain of femtoseconds by means of a fluorescence up-conversion method (pulse width, 80 fs) [23].

2.2. MDS calculations

The starting structure of the pig kidney DAAO monomer was obtained from using the X-ray structure of the DAAO-benzoate complex dimer (PDB code 1VE9) [10], removing benzoate and/or one of the subunits. All calculations were carried out using the AMBER 10 suite of programs [47]. The parm99 force field [48] was used to describe the protein atoms, whereas the general AMBER force field [49] with the restrained electrostatic potential (RESP) charges [50] was used for the ligand and FAD. The simulated systems were subsequently solvated with a cubic box of ca. 4000 TIP3P water molecules. Electrostatic interactions were corrected by the

particle mesh Ewald method [51]. The SHAKE algorithm [52] was employed to constrain all bonds involving hydrogen atoms. Details of the methods are described elsewhere [53–56].

2.3. Method of ET analysis

2.3.1. ET theory

The original Marcus theory [57–59] has been modified in various ways [60–73]. Kakitani and Mataga (KM) theory [66–68] is used for ET phenomena in flavoproteins, because it is applicable both for adiabatic and nonadiabatic ET process and has been found to give satisfactory results for both static [26–30] and dynamic ET analyses [31–36].

Here, the ET rate with the KM model for the DAAO dimer [53] is described as expressed by Eq. (3). The rates are similar for other DAAOs and DAOBs:

$$k_{ET}^{jk}(T) = \frac{v_0^q}{1+\exp\left\{\beta^q\left(R_{jk}-R_0^q\right)\right\}}\sqrt{\frac{k_BT}{4\pi\lambda_{jk}^q}}\exp\left[-\frac{\left\{\Delta G_k^0(T)-e^2/\varepsilon_0^{pk}R_{jk}+\lambda_{jk}^q+E_{Net}^k(j)\right\}^2}{4\lambda_{jk}^q k_BT}\right] \quad (3)$$

where $k_{ET}^{jk}(T)$ is the ET rate from the donor j to the Iso* in subunit k (k = Sub A or Sub B) at temperature T (°C), and q denotes Trp or Tyr. The term v_0^q is an adiabatic frequency, β^q is the ET process coefficient, and R_{jk} and R_0^q are the donor j-Iso distance in subunit k and its critical distance for the ET process, respectively, and are expressed with Rc (center-to-center distance). The ET process is adiabatic when $R_{jk} < R_0^q$ and nonadiabatic when $R_{jk} > R_0^q$. The temperature (T) is expressed in K unit at the right-hand side. The term $-e^2/\varepsilon_0^{pk}R_{jk}$ is the electrostatic (ES) energy between the donor cation and acceptor anion (ESDA), in which ε_0^{pk} is static dielectric constant. The terms k_B and e are the Boltzmann constant and electron charge, respectively. $E_{Net}^k(j)$ is the net ES (NetES) energy of the donor j in subunit k. The DAAO monomer contains 10 Trp and 14 Tyr residues. In the present work, the ET rates from all of these aromatic amino acids to Iso* are taken into account for the analysis.

Solvent reorganization energy (SROE) [57, 58] of the ET donors q and j (λ_{jk}^q) is expressed in Eq. (4):

$$\lambda_{jk}^q = e^2\left(\frac{1}{2a_{Iso}}+\frac{1}{2a_q}-\frac{1}{R_{jk}}\right)\left(\frac{1}{\varepsilon_\infty}-\frac{1}{\varepsilon_0^{pk}}\right) \quad (4)$$

where a_{Iso} and a_q are the radii of Iso and Trp or Tyr, ε_∞ is the optical dielectric constant, and ε_0^{pk} is the static dielectric constant inside subunit k. The optical dielectric constant used was 2.0. The radii of Iso (a_{Iso}), Trp (a_{Trp}), and Tyr (a_{Tyr}) are 0.224, 0.196, and 0.173 nm, respectively, as previously reported [26–36].

The standard free energy gap (SFEG) between the products and reactants, $\Delta G_k^0(T)$, was expressed with the ionization potential of the ET donor (E_{IP}^q) as in Eq. (5):

$$\Delta G_k^0(T) = E_{IP}^q - G_k^0(T) \tag{5}$$

where $G_k^0(T)$ is the standard free energy gap related to the electron affinity of Iso* in subunit k at temperature T. The values of E_{IP}^q for Trp and Tyr are 7.2 eV and 8.0 eV, respectively [74].

2.3.2. Electrostatic energy between the photoproducts and ionic groups inside the DAAO dimer

The FAD cofactor in DAAO has two negative charges at the pyrophosphate, while DAAO itself contains 22 Glu, 13 Asp, 12 Lys, and 21 Arg residues per subunit as ionic amino acids. The ES energy between the Iso anion or donor cation j and all other ionic groups in subunit k (Sub A or Sub B) is expressed by Eq. (6):

$$\begin{aligned} E_k(j) = &\sum_{i=1}^{44} \frac{C_j C_{Glu}}{\varepsilon_0^{pk} R_j(Glu - i)} + \sum_{i=1}^{26} \frac{C_j C_{Asp}}{\varepsilon_0^{pk} R_j(Asp - i)} + \sum_{i=1}^{24} \frac{C_j C_{Lys}}{\varepsilon_0^{pk} R_j(Lys - i)} \\ &+ \sum_{i=1}^{42} \frac{C_j C_{Arg}}{\varepsilon_0^{pk} R_j(Arg - i)} + \sum_{i=1}^{8} \frac{C_j C_P}{\varepsilon_0^{pk} R_j(P - i)} \end{aligned} \tag{6}$$

Here, $j = 0$ is for the Iso anion in subunit k, 1–10 and 11–20 for the Trp cations in Sub A and Sub B, respectively, and 21–34 and 35–48 for the Tyr cations in Sub A and Sub B, respectively. The charge of the aromatic ionic species j (C_j) is -e for $j = 0$ (Iso anion) and +e for j = 1–48 (cations of the donors). C_{Glu} (= $-e$), C_{Asp} (= $-e$), C_{Lys} (= + e), and C_{Arg} (= + e) are the charges of the Glu, Asp, Lys, and Arg residues, respectively. FAD contains two phosphate atoms, each of which binds two oxygen atoms, where the charge of each oxygen atom is $C_P = -0.5e$ and so the total charge of four oxygen atoms is $-2e$. The distances between the aromatic ionic species j and the i^{th} Glu (i = 1–44) were denoted as $R_j(Glu - i)$, while the distances between the aromatic ionic species j^{th} and the i^{th} Asp (i = 1–26) were denoted as $R_j(Asp - i)$ and so on for the each amino acid residue. The NetES in Eq. (3) is then expressed as in Eq. (7):

$$E_{Net}^k(j) = E_k(0) + E_k(j) \tag{7}$$

where j ranges from 1 to 48 and represents the j^{th} ET donor.

2.3.3. Determination of the ET parameters

The calculated lifetimes of subunit k at temperature *(T)* are given by Eq. (8):

$$\tau_{Calc}^{Tk} = \frac{1}{\sum_{j=1}^{48} k_{ET}^{jk}(T)} \tag{8}$$

where the fluorescence lifetimes are expressed in ps unit. The physical quantities related to the electronic coupling term (υ_0^q, β^q, and R_0^q) for Trp and Tyr are taken from those reported for flavin mononucleotide binding proteins [32] and are assumed to be independent of temperature within the 10–30°C temperature range. In contrast, the free energy, $G_k^0(T)$, which is related to the electron affinity of Iso*, is assumed to be both temperature and subunit dependent,

because $G_k^0(T)$ may be modified with the H-bond structure. The unknown ET parameters are $G_A^0(10)$, $G_B^0(10)$, $G_A^0(30)$, and $G_B^0(30)$ in Eq. (5) and ε_0^A, ε_0^B, and ε_0^{DA}, which are assumed to be independent of temperature. These ET parameters are determined so as to obtain the minimum value of χ^2, as given by Eq. (9):

$$\chi^2 = \frac{\left(\tau_{Calc}^{10A} - \tau_{Obs}^{10}\right)^2}{\tau_{Calc}^{10A}} + \frac{\left(\tau_{Calc}^{10B} - \tau_{Obs}^{10}\right)^2}{\tau_{Calc}^{10B}} + \frac{\left(\tau_{Calc}^{30A} - \tau_{Obs}^{30}\right)^2}{\tau_{Calc}^{30A}} + \frac{\left(\tau_{Calc}^{30B} - \tau_{Obs}^{30}\right)^2}{\tau_{Calc}^{30B}} \tag{9}$$

3. Cooperative binding of FAD associated with the monomer-dimer equilibrium in DAAO

The DAAO exists in a monomer (Mw 39 kDa)-dimer equilibrium state at relatively low concentrations [75–79] and in a dimer-tetramer equilibrium at higher concentrations [80–82]. The protein structures of the DAAO dimer in solution, as obtained by MDS [53, 54], are shown in **Figure 1**. The values of K_d are obtained at various concentrations of holo-DAAO and apo-DAAO [42, 43] according to Eq. (1). **Figure 2** shows K_d vs. DAAO concentration relationship [42]. The values of K_d are remarkably dependent on the protein concentration both in holo-DAAO and apo-DAAO [42], higher at the low concentrations and lower at the high concentrations. **Figure 3**

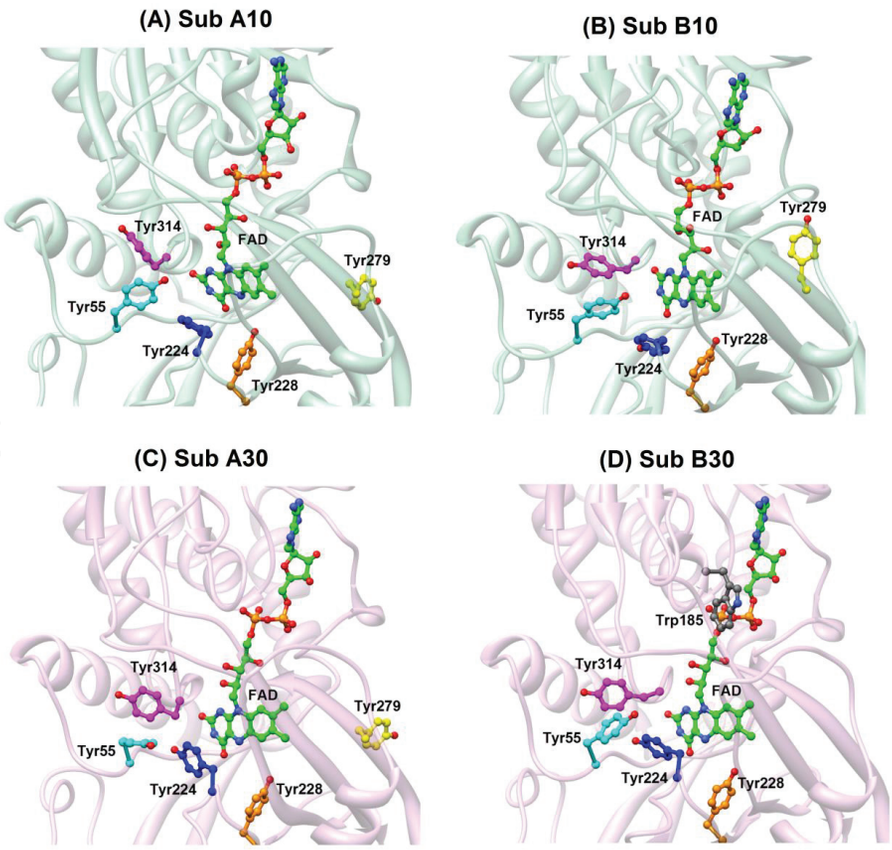

Figure 1. Structure of FAD binding site in holo-DAAO dimer obtained by MDS. (A) Sub A10 and (B) Sub B10 denote subunits of A and B at 10°C, and (C) Sub A30 and (D) Sub B30 denote subunits of A and B at 30°C. (Reproduced from [53] with permission from the PCCP Owner Societies).

http://dx.doi.org/10.5772/intechopen.68645

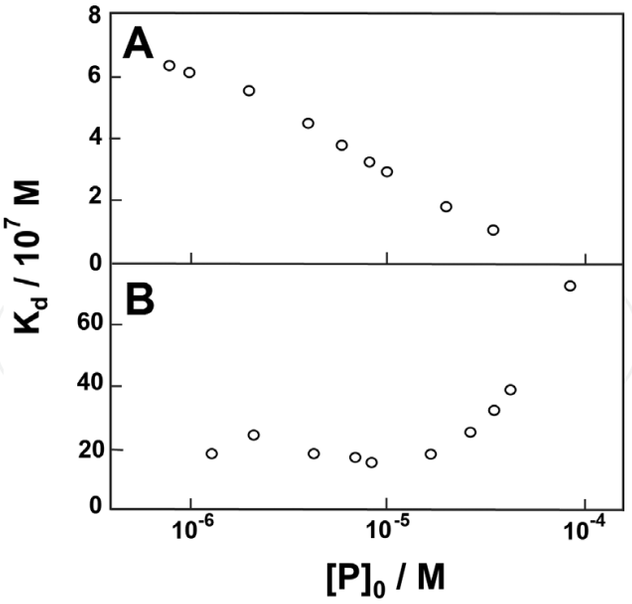

Figure 2. Dependence of K_d on the concentration of DAAO. (A) shows the holo-DAAO and (B) apo-DAAO. DAAO was dissolved into buffer solution at pH 8.3. (Reprinted with permission from [42]. Copyright (1979) American Chemical Society).

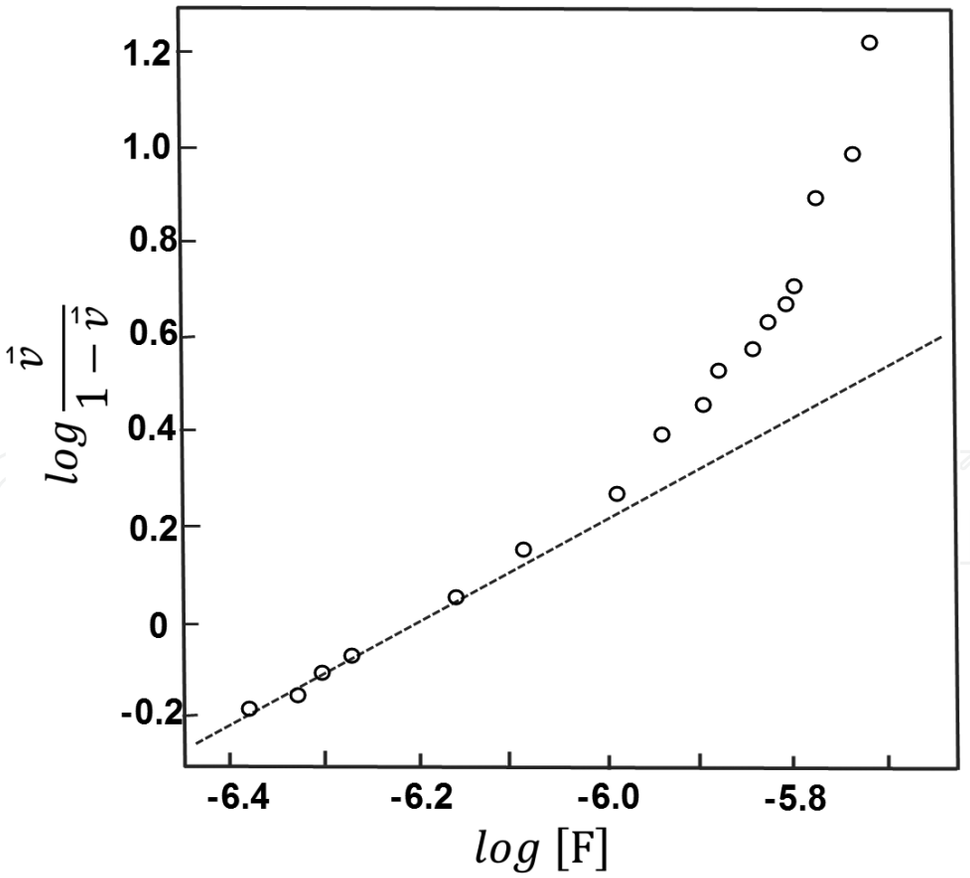

Figure 3. Hill plot of FAD binding in holo-DAAO. Measurements were made at pH 8.3 and 20°C. The binding fraction of FAD is $\bar{\nu} = [F]_b/[P]_0$ where $[F]_b$ is the concentration of bound FAD. The dashed line indicates a straight line with the Hill coefficient equal to 1. (Reprinted with permission from [42]. Copyright (1979) American Chemical Society).

shows Hill plot for FAD binding, which reveals that the Hill coefficient is nearly 1 at the lower concentrations but appreciably deviates from 1 toward greater than 1 at the higher concentrations of DAAO [42]. The results show that the binding process of FAD is positively cooperative. Approximate relative concentrations of various species of DAAO and the dissociation constants are illustrated in **Figure 4** [42]. The origin of the cooperativity is elucidated to be mainly that Kc (0.01 μM) is much less than Ka (0.74 μM). Namely, the binding of FAD to apo-DAAO monomer induces association of the holo-DAAO monomers into the holo-DAAO dimer, because the protein dissociation constants between holo monomers (K_2 = 3.8 μM) are least comparing to the other protein dissociation constants (K_1 and K_0).

The concept of "allosteric transition" is originally proposed by Monod, Wyman, and Changeux to explain the sigmoidal curve of O_2 binding to hemoglobin [83]. Then, an induced-fit model for the O_2 binding is proposed by Koshland, Némethy, and Filmer [84]. A ligand-induced polymerization of a protein is considered as an alternative model to explain allosteric effect [85–87]. The enzyme activity of the DAAO monomer is 1.5-fold higher than that of the dimer [88]. Under the presence of enough FAD in the brain, DAAO is considered to form the dimer, for which activity is lower than that of the monomer. The enzyme activity may be physiologically regulated through the binding of FAD, which should be significant in schizophrenia, because the activity of DAAO is twofold higher in the patients with schizophrenia [7].

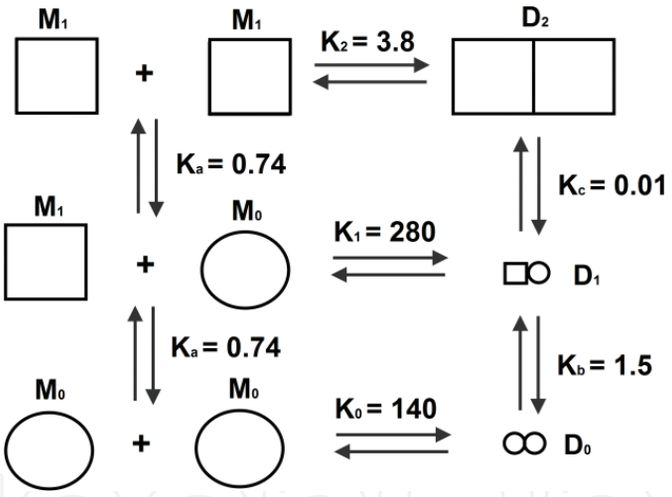

Figure 4. Dissociation equilibrium constants among the various species of DAAO. M_1 and M_0 indicate holomonomer and apomonomer, and D_2, D_1, and D_0 indicate holodimer, heterodimer of holo- and apomonomers, and apodimer, respectively. Ka, Kb, and Kc are dissociation equilibrium constants of FAD from holomonomer, heterodimer, and holodimer, respectively. The dissociation constants are indicated in the unit of μM. The square binds FAD, while the circle has no FAD. The concentration of DAAO is 5 μM. The area of the various species is approximately proportional to their concentrations. (Reprinted with permission from [42]. Copyright (1979) American Chemical Society).

4. Fluorescence lifetimes of DAAO and DAOB in picoseconds-femtoseconds time domain

The dissociation constants of FAD in DAAO are much smaller by 1/74 in the dimer, comparing to the monomer [42, 43] as stated above. This suggests that local structures near Iso binding site are different between the dimer and monomer. The fluorescence lifetimes of

DAAO obtained by Nakashima et al. [44] are 40 ps in the dimer and 130 ps in the monomer. Later, the lifetimes were measured with the new method of single-photon counting instruments and listed in **Table 1** at various concentrations of DAAO and temperatures [46, 47]. The values of lifetimes in DAAO monomer are 228 ps at 10°C and 182 ps at 30°C. The values of the lifetime in the dimer are 44.2 ps at 10°C and 37.7 ps at 30°C [46]. The lifetime of free FAD in water is 2.5 ns [15, 16]. The lifetime in DAAO dimer is shorter by ca. 1/60 times than that in free FAD in water, which is ascribed to fast ET from aromatic amino acids to Iso* [19–21].

The fluorescence lifetime of DAOB is 60 ps in the monomer, and shorter than 5 ps in the dimer, obtained by Nakashima et al. [44]. Time resolution of the lifetime instruments in 1980 was not enough to obtain exact lifetime of DAOB dimer. In 2000 the lifetimes of the DAOB dimer are obtained to be 0.848 and 4.77 ps [23] by means of the up-conversion method, which are much shorter than those in DAAO, and described more in detail later.

T (°C)	Conc. (μM)	τ_0 (ps)	α_0	τ_1 (ps)	α_1	τ_2	α_2	τ_3 (ns)	α_3	χ^2
40	1.6	27.9	−0.877	43.7	0.850	191	0.079	1.91	0.071	1.028
	100	26.5	−0.962	36.2	0.945	162	0.047	1.61	0.008	1.362
	Av.	25.9		40.0		169		1.76		
35	0.78	26.2	−1.030	45.4	0.834	202	0.084	2.10	0.081	0.993
	100	23.5	−0.903	39.9	0.910	161	0.080	1.68	0.010	1.516
	Av.	25.6		41.8		170		1.91		
30	1.6	26.7	−0.989	48.3	0.824	182	0.116	2.23	0.060	1.007
	100	26.7	−1.024	37.7	0.956	169	0.044	1.76	0.005	1.479
	Av.	26.2		43.2		177		2.02		
25	0.78	28.6	−0.842	54.7	0.822	245	0.080	2.47	0.098	1.148
	100	23.5	−0.977	41.0	0.906	165	0.086	1.83	0.008	1.559
	Av.	26.0		43.7		184		2.20		
15	0.78	29.5	−0.841	46.6	0.822	214	0.110	2.78	0.068	1.134
	100	23.5	−1.003	42.9	0.892	179	0.099	1.95	0.009	1.324
	Av.	26.1		45.2		190		2.44		
10	0.78	27.6	−0.980	47.1	0.807	228	0.121	2.93	0.072	1.016
	100	25.3	−0.979	44.2	0.899	194	0.092	2.04	0.009	1.366
	Av.	25.1		48.5		208		2.61		

[a]DAAO was dissolved in 0.017 M pyrophosphate buffer at pH 8.3. The fluorescent species with the lifetimes, τ_1, τ_2, and τ_3, were assigned to be the dimer, monomer, and free FAD, respectively, and α_1, α_2, and α_3 are their fractions. τ_0 is a lifetime for process from an intermediate state to the fluorescent state [46, 47]. χ^2 means a reduced chi-square distribution between the calculate decay function and experimental decay curve. Av. indicates the averaged lifetimes over seven or eight different levels of the enzyme ranging from 100 to 1.6 or 0.78 M. (Reprinted with permission from [47]).

Table 1. Fluorescence decay parameters of FAD in DAAO measured with a synchronously pumped, cavity-dumped dye laser and single-photon counting system.[a].

5. Conformational difference between the DAAO dimer and monomer revealed by MDS and ET analyses

The results of the fluorescence lifetimes of DAAO and DAOB reveal that the local structures differ between the monomers and dimers. However, no structural information can be drawn by the lifetimes alone. Details of the structural difference between DAAO monomer and dimer are obtained through MDS and ET analyses [53, 54].

Table 2 lists the donor-acceptor distances between Iso and the five shortest donors from Iso in the DAAO dimer and monomer. In the dimer, the Rc distances are the shortest in Tyr224 followed by Tyr228, except for Sub A at 30°C where Tyr228 is the shortest followed by Tyr224. In the monomer

Protein	T (°C)	Subunit	Donor [b] (Rc/nm)					
DAAO dimer[c]	10	A	Tyr224	Tyr228	Tyr55	Tyr314	Tyr279	
			(0.74)	(0.82)	(1.07)	(1.11)	(1.32)	
	10	B	Tyr224	Tyr228	Tyr55	Tyr314	Tyr279	
			(0.79)	(0.83)	(0.99)	(1.05)	(1.20)	
	30	A	Tyr 228	Tyr 224	Tyr 314	Tyr 279	Tyr 55	
			(0.85)	(0.90)	(1.06)	(1.30)	(1.47)	
	30	B	Tyr 224	Tyr 228	Tyr 314	Tyr 55	Trp 185	
			(0.72)	(0.81)	(1.06)	(1.06)	(1.14)	
DAAO monomer[d]	10		Tyr224	Tyr228	Tyr314	Trp185	Tyr55	
			(0.82)	(0.88)	(1.06)	(1.27)	(1.64)	
	30		Tyr224	Tyr228	Tyr314	Tyr55	Trp185	
			(0.88)	(0.88)	(1.18)	(1.20)	(1.49)	
DAOB dimer[e]	20	A	Tyr55	Tyr228	Tyr314	Trp185	Tyr224	Benzoate
			(0.95)	(0.96)	(1.06)	(1.10)	(1.32)	(0.66)
	20	B	Tyr228	Tyr314	Tyr224	Tyr55	Trp185	Benzoate
			(0.99)	(1.02)	(1.04)	(1.05)	(1.31)	(0.68)
DAOB monomer[f]	20		Tyr228	Tyr224	Tyr314	Tyr279	Tyr74	Benzoate
			(0.81)	(0.97)	(1.07)	(1.24)	(1.80)	(0.61)

[a]The ET acceptor is Iso*. Mean donor-acceptor distances (Rc) are listed over 5000 snapshots in parentheses. A value of Rc in one snapshot was evaluated as mean distance of all possible pairs between aromatic atoms in Iso and aromatic atoms in a donor.
[b]Five shortest distances between Iso and the aromatic amino acids (plus Bz in DAOB) are listed in order from shorter to longer distances.
[c]Data taken from Ref. [53].
[d]Data taken from Ref. [54].
[e]Data taken from Ref. [56].
[f]Data taken from Ref. [55].

Table 2. ET donor-acceptor distance in DAAO and DAOB.[a].

the distance is also the shortest in Tyr224 at both 10 and 30°C, followed by Tyr228 and Tyr314. The hydrogen bonding (H-bond) structures between Iso and the amino acid residues markedly vary with the protein systems (**Table 3**). At 10°C, in the dimer Iso forms H-bonds with Leu51 (IsoN3H), Thr317 (IsoO2), Gly50 (IsoO4), and Leu51 (IsoO4) in Sub A and with Gly315 (IsoO2), Leu316 (IsoO2), and Thr317 (IsoO2) in Sub B (atom notations are shown in **Chart 1**), while in the monomer, Iso forms H-bond only with Gly50 (IsoO4). At 30°C Iso in the dimer forms H-bonds with Leu51 (IsoN3H) and Thr317 (IsoO2) in Sub A and with Gly315 (IsoO2), Leu316 (IsoO2), and Thr317 (IsoO2) in Sub B, while in the monomer, Iso forms H-bond with Leu316 (IsoO2) and Gly50 (isoO4). The number of H-bonds and kind of H-bond pairs are quite different between the DAAO dimer and monomer, though Iso may also form H-bonds with water molecules as described below.

Protein	Subunit	T (°C)	Iso N3H Leu51 (O)	Iso N5 Ala49 (N)	Iso O2 Gly315 (N)	Iso O2 Leu316 (N)	Iso O2 Thr317 (OG1)	Iso O4 Gly50 (N)	Iso O4 Leu51 (N)
DAAO	A[b]	10	0.29	-	-	-	0.28	0.29	0.29
		30	0.29	-	-	-	0.28	-	-
	B[b]	10	-	-	0.29	0.28	-	-	-
		30	-	-	0.29	0.28	-	-	-
	Monomer[c]	10	0.29	0.29	-	0.29	0.28	0.28	0.29
		30	-	0.29	-	0.28	0.28	0.28	-
DAOB	A[d]	20	0.31	0.31	-	-	0.35	-	-
	B[d]		0.32	0.31	-	-	-	-	-
	Monomer[e]	10	0.29	0.29	-	0.29	0.28	0.28	0.29
		20	0.29	0.29	0.29	-	0.28	-	-
		30	0.29	0.29	-	-	-	0.28	0.29

	Subunit	T (°C)	Bz O1 Arg283 (NH2)	Bz O2 Arg283 (NE)	Bz O2 Arg283 (NH2)
DAOB	A[d]	20	0.29	0.27	0.30
	B[d]		0.28	0.28	0.30
	Monomer[e]	10	0.28	0.28	0.29
		20	0.26	0.28	0.29
		30	0.28	0.28	0.28

[a]The distances in nm units are obtained by averaging over 10,000 MDS snapshots and collected those shorter than 0.3 nm. Atomic notations in Iso are indicated in **Chart 1**. Atom notations of amino acids shown in parentheses are taken from PDB, where N, O, and OG1 denote peptide N and O atoms and O atom of the side chain, respectively. Bz O1 and Bz O2 denote two oxygen atoms of carboxylate in benzoate (Bz).
[b]The data are taken from Ref. [53].
[c]The data are taken from Ref. [54].
[d]The data are taken from Ref. [56].
[e]The data are taken from Ref. [55].

Table 3. Comparison of H-bond distances among the DAAO dimer, monomer, and DAOB dimer and monomer.[a].

As shown in Eq. (3), the ET rate contains several parameters, which are determined by the method described above. **Table 4** lists the ET parameters as ε_0^{DA} and $G_k^0(T)$ in DAAO dimer (Sub A and Sub B), DAAO monomer, DAOB dimer (Sub A and Sub B), and DAOB monomer. Microscopic information can be obtained as the donor-acceptor distances and H-bond distances with MDS and the protein structures. Submicroscopic information can be obtained with the ET parameters, ET rates, and related physical quantities. Among the ET parameters, $G_k^0(T)$ is one of most influential parameters for the ET rate, according to the fluorescence lifetime.

The distribution of the logarithmic ET rates (ln rate) from the five fastest donors to Iso* in the DAAO dimer and monomer is shown in **Figure 5**. At 10°C the three fastest donors are Tyr224, Tyr314, and Tyr228 in Sub A in this order and Tyr314, Tyr224, and Tyr55 in Sub B in the dimer, while they are Tyr224, Tyr314, and Tyr228 in the monomer. At 30°C the three fastest donors are Tyr314, Tyr228, and Tyr224 in Sub A and Tyr224, Tyr314, and Trp185 in Sub B in the dimer, while they are Tyr314, Tyr224, and Tyr55 in the monomer. The values of ET rates are listed in **Table 5**. The ET rates in the dimer are several times faster than those in the monomer.

T (°C)	Protein	Subunit	ε_0^{DA} [b]	$G_k^0(T)$ [c] (eV)	τ (ps)	
					Obs [d]	Calc [e]
10	DAAO dimer[f]	Sub A	5.79	8.61	44.2	44.2
		Sub B	5.82	8.54	-	-
	DAAO monomer[f]	–	5.88	8.69	228	228
30	DAAO dimer[f]	Sub A	5.79	8.73	37.7	37.7
		Sub B	5.82	8.48	-	-
	DAAO monomer[f]		5.89	8.51	182	182
20	DAOB dimer[g]	Sub A	2.53	8.42	4.77	4.77
		Sub B	2.64	8.43	0.848	0.848
	DAOB monomer[h]	-	2.45	8.53	60	60

[a]Static dielectric constants inside the proteins (ε_0^A and ε_0^B) are similar, 5.8–5.9 among all species. The reported values of ET parameters were used for the electronic coupling term ($\nu_0^{Trp} = 1016\ \text{ps}^{-1}$, $\nu_0^{Tyr} = 197\ \text{ps}^{-1}$, $\beta^{Trp} = 21.0\ \text{nm}^{-1}$, $\beta^{Tyr} = 6.25\ \text{nm}^{-1}$, $R_0^{Trp} = 0.663$ nm, and $R_0^{Tyr} = 0.499$ nm) [32].
[b]The static dielectric constant between Iso and the donors within 1 nm from Iso.
[c]Temperature-dependent electron affinity of Iso*.
[d]Experimental fluorescence lifetimes for DAAO dimer and monomer [46] and for DAOB dimer [23] and DAOB monomer [45]. The lifetimes of Sub A and Sub B in DAAO dimer are not experimentally resolved.
[e]Calculated lifetimes.
[f]Data are taken from the work for DAAO dimer [53] and DAAO monomer [54].
[g]Data are taken from the reported work of Ref. [56].
[h]Data are taken from the reported work of Ref. [55].

Table 4. ET parameter in DAAO and DAOB.[a].

http://dx.doi.org/10.5772/intechopen.68645

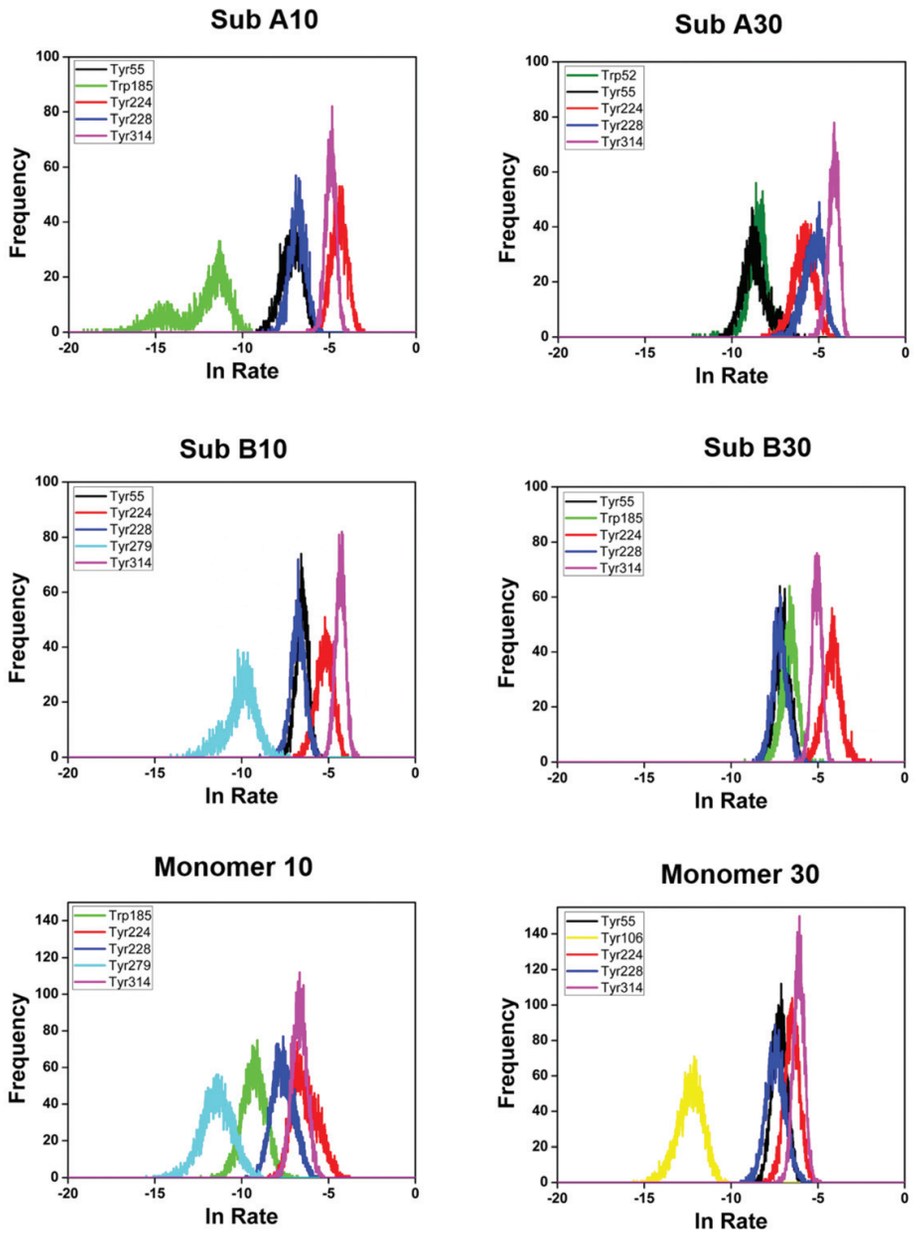

Figure 5. Distribution of logarithmic ET rate from aromatic amino acids to Iso*. Sub A10 and Sub B10 denote Sub A and Sub at 10°C, and Sub A30 and Sub B30 denote Sub A and Sub B at 30°C in DAAO dimer, respectively. Inserts show amino acids with the top fastest ET rates. The distributions for DAAO monomers at 10°C (Monomer 10) and 30°C (Monomer 30) are also shown for comparison. The kinds of the amino acids are different among the six groups including monomer. (Reproduced from [53] with permission from the PCCP Owner Societies).

A NetES sometimes plays an important role on the ET rates and is defined as an ES energy between the photoproducts (Iso anion plus a donor cation), and other ionic groups in the protein [31–36] as described above are also listed in **Table 5**. The NetES has never been numerically evaluated by other research groups. The NetES values in the monomer are greatly modified upon the formation of dimer, which is ascribed to inter-subunit interactions, namely, that the NetES of a donor in Sub A is strongly influenced by that in Sub B and vice versa, because the electrostatic energy is influential over a long range.

Protein	T (°C)	Subunit	Donor	Rate (ps^{-1})	NetES energy (eV)
DAAO dimer[b]	10	A	Tyr224	1.29×10^{-2}	0.044
			Tyr314	7.57×10^{-3}	−0.406
			Tyr228	1.20×10^{-3}	0.146
			Tyr55	9.08×10^{-4}	−0.119
			Trp185	9.71×10^{-6}	−0.104
	10	B	Tyr314	1.38×10^{-2}	−0.479
			Tyr224	5.96×10^{-3}	−0.021
			Tyr55	1.54×10^{-3}	−0.161
			Tyr228	1.25×10^{-3}	0.056
			Tyr279	6.08×10^{-5}	−0.076
	30	A	Tyr314	1.63×10^{-2}	−0.293
			Tyr228	5.86×10^{-3}	0.130
			Tyr224	3.39×10^{-3}	0.108
			Tyr55	2.43×10^{-4}	−0.207
			Trp52	2.15×10^{-4}	−0.593
	30	B	Tyr224	1.68×10^{-2}	−0.038
			Tyr314	6.51×10^{-3}	−0.422
			Trp185	1.43×10^{-3}	−0.465
			Tyr55	9.70×10^{-4}	−0.210
			Tyr228	8.30×10^{-4}	0.097
DAOB dimer[d]	20	A	Tyr228	1.17×10^{-1}	0.075
			Bz	7.50×10^{-2}	−0.085
			Tyr55	1.14×10^{-2}	−0.103
			Trp185	4.65×10^{-3}	−0.434
			Tyr314	1.58×10^{-3}	−0.323
			Trp52	1.68×10^{-5}	−0.113
	20	B	Bz	8.92×10^{-1}	−0.094
			Tyr228	2.80×10^{-1}	0.070
			Tyr314	6.56×10^{-3}	−0.442
			Tyr55	2.64×10^{-4}	−0.159
			Tyr224	5.38×10^{-5}	−0.010
			Trp185	3.72×10^{-5}	−0.183
DAAO monomer[c]	10		Tyr224	2.27×10^{-3}	0.192
			Tyr314	1.38×10^{-3}	−0.073
			Tyr228	5.94×10^{-4}	0.215
			Trp185	1.15×10^{-4}	−0.249

Protein	T (°C)	Subunit	Donor	Rate (ps^{-1})	NetES energy (eV)
			Tyr279	1.57×10^{-5}	0.144
	30		Tyr314	2.35×10^{-3}	−0.434
			Tyr224	1.65×10^{-3}	−0.035
			Tyr55	8.00×10^{-4}	−0.324
			Tyr228	6.85×10^{-4}	0.051
			Tyr106	5.47×10^{-6}	−0.342
DAOB monomer[e]	20		Bz	9.92×10^{-3}	0.898
			Tyr228	4.23×10^{-3}	0.172
			Tyr224	1.93×10^{-3}	0.022
			Tyr314	5.05×10^{-4}	−0.130
			Tyr55	6.59×10^{-5}	−0.171
			Trp185	1.37×10^{-5}	−0.095

[a]Mean ET rates from aromatic amino acids to Iso* and related physical quantities are listed over 10,000 snapshots. The expression of ET rate with KM model is given by Eq. (3). NetES energy denotes electrostatic energy between the photoproducts (Iso anion and a donor cation) and other ionic groups in the proteins given by Eq. (7).
[b]The data are taken from Ref. [53].
[c]The data are taken from Ref. [54].
[d]The data are taken from Ref. [56].
[e]The data are taken from Ref. [55].

Table 5. Comparison of ET rate and NetES energy among DAAO dimer and monomer and DAOB dimer and monomer.[a].

The dependence of the ln Rate on the donor-acceptor distances has been predicted by a Dutton rule to be linear [69]. In DAAO dimer and monomer, the ln Rate linearly decreased with Rc in all cases [53, 54]. This means that the fluorescence lifetimes of FAD in DAAO become longer as the Rc increased. The dimer Rc is mostly shorter than those in the monomer [53]. It is concluded that the shorter lifetimes of the dimer are due to their shorter Rc values compared to the monomer.

6. The two subunits in the DAAO dimer are not equivalent in solution

The conformations of the two subunits in the DAAO dimer are found to be not equivalent in solution [53], as shown in **Figure 1**. The Rc values in Sub A between Iso and the main donors are quite different from those in Sub B (**Table 2**), and the H-bond structure between Iso and the nearby amino acids in Sub A is also quite different from that in Sub B (**Table 3**), though H-bonds between Iso and water molecules are not taken into account. The structural differences led to the nonequivalent ET rate and NetES (**Table 5**), and its related physical quantities as the electrostatic energy between the donor and acceptor (ESDA), and solvent reorganization energy (SROE). The ratio of the ET rate in Sub A/the rate in Sub B is 2.3 in Tyr224, 0.55 in Tyr314, and 0.96 in Tyr228 at 10°C and 0.20 in Tyr224, 2.5 in Tyr314, and 7.1 in Tyr228 at 30°C.

7. Temperature-induced structural transition in DAAO monomer

Massey et al. [39] first reported a temperature-induced conformational change (temperature transition) of DAAO, where the tryptophan fluorescence exhibited a temperature transition at around 15°C. The van't Hoff plot of the enzyme activity is nonlinear and best expressed by two straight lines with different activation energies. The enzyme activities showed a temperature-dependent equilibrium between the high- and low-temperature states [89], while the equilibrium constant of the association of monomers to form dimers exhibited a discontinuous change at 18°C [88]. However, this transition is not found in the specific heat change at the transition temperature by means of a differential scanning microcalorimetry [90]. The temperature transition of DAAO has been studied by monitoring the fluorescence lifetimes [46]. The modified Arrhenius plots of the fluorescence quenching constants of the monomer and dimer based upon the absolute rate theory displayed two linear functions both in the monomer and dimer. The fluorescence quenching in DAAO is ascribed to the ET from aromatic amino acids to Iso* [19–21], as described above. The activation enthalpy gap and the entropy gap for the quenching constants of DAAO displayed different values in the lower and higher temperature ranges than at 16–18°C, but not in the free FAD. The quenching constant of the monomer displayed a more pronounced transition than that of the dimer. No indication of appreciable transition in the specific heat change [90] may be due to the measurements being performed at very high concentrations of DAAO, where the enzyme should be in the dimer or higher association state, and so it might be difficult to detect the transition.

The structural basis for the temperature-induced transition in the DAAO monomer is studied by means of MDS and ET analyses [54]. The Rc values of Tyr224 are 0.82 and 0.88 nm at 10 and 30°C, respectively, and those of Tyr314 are 1.06 and 1.18 nm at 10 and 30°C, respectively, as shown in **Table 2**. H-Bonds are formed between IsoN1 (see **Chart 1** for atom notations of Iso ring) and Gly315N (peptide), between IsoN3H and Leu51O (peptide), and between IsoN5 and

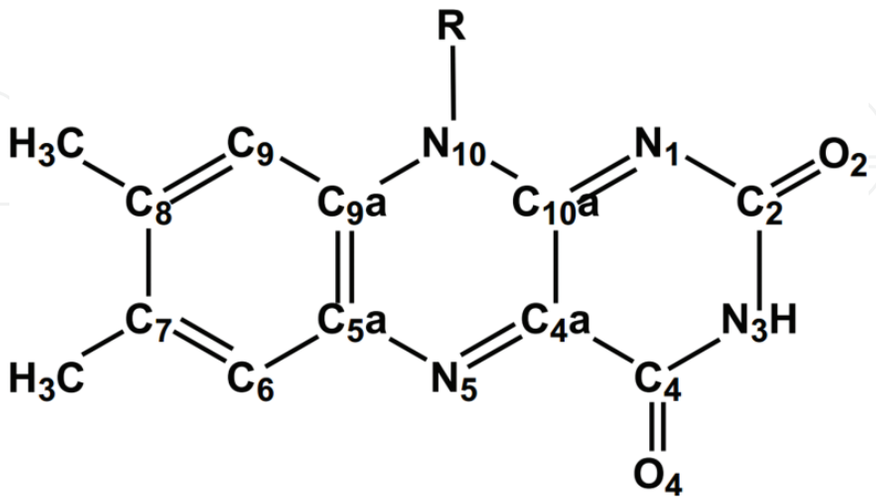

Chart 1. Chemical structure and atom notations of Iso.

Ala49N (peptide) at 10°C, while no H-bond is formed at IsoN1 and IsoN3H at 30°C (**Table 3**). The H-bond of IsoO4 with Leu51N (peptide) at 10°C is switched to Ala49N (peptide) at 30°C. These results may account for the shorter reported fluorescence lifetime of the monomer at 10°C (228 ps) and 30°C (182 ps) [54]. The ET rate from Tyr224 is the fastest among donors at 10°C and the second fastest at 30°C among the donors, while that from Tyr314 is the second fastest at 10°C and the fastest at 30°C (see **Table 5**). The values of NetES in Tyr224 are 0.192 eV at 10°C and −0.035 eV at 30°C, and in Tyr314 are −0.073 eV at 10°C and −0.434 eV at 30°C. The other physical quantities related to the ET rates also displayed appreciable differences at 10 and 30°C. The electron affinities of Iso* are calculated at both temperatures with the semiempirical molecular orbital (MO) method (MOPAC software, PM6 basis set) [54]. The mean calculated electron affinities over 100 snapshots with 0.1 ns intervals are 7.69 eV at 10°C and 7.59 eV at 30°C. Thus, the difference in the observed fluorescence lifetimes between 10 and 30°C is ascribed to the differences in the standard free energy gap and also NetES between the two temperatures.

8. Comparison of the DAOB monomer and dimer structures

Characteristics of monomer and dimer in DAOB and DAAO are compared in **Table 6**.

The Rc values between Iso and Bz are 0.61 nm in the DAOB monomer but 0.66 and 0.68 in Sub A and Sub B, respectively [55, 56], of the dimer as shown in **Table 2**. In the DAOB monomer, the second and third shortest donors are Tyr228 and Tyr224 (0.81 and 0.97 nm,

Physical quantity	DAOB	DAAO
Fluorescence lifetime (ps)		
Monomer	60[b]	130[c], 228 at 10°C[d], 182 ps at 30°C[d]
Dimer	4.8[e]	40[c], 44.2 at 10°C[d], 37.7 at 30°C[d]
Sub A	0.85[e]	
Sub B		
Relative quantum yield of FAD in the enzyme to free FAD [e]	0.0048–0.0077[f]	0.08–0.13[c]
Apparent dissociation constant of FAD (nm)	0.14–0.15[f]	100–300[f]
Dissociation constant of dimer into monomer (μM)	0.4 ± 0.3[f]	3.7[g]

[a]Data are taken with some modifications from [45]. The lifetimes of the DAAO dimer were not separated between the two subunits [44, 46].
[b]Temperature was 20°C. Data are taken from Ref. [45].
[c]Temperature was 20°C. Data are taken from Ref. [44].
[d]Data are taken from Ref. [46].
[e]Data are taken from Ref. [23].
[f]Data are taken from Ref. [45].
[g]Data are taken from Ref. [42, 43].

Table 6. Comparison of characteristics among DAAO monomer and the dimer and DAOB monomer and the dimer.[a].

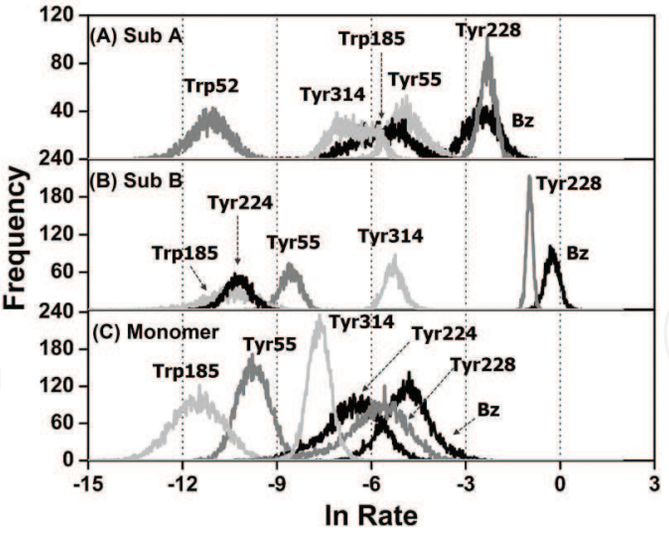

Figure 6. Comparison of the distribution of ln Rate between DAOB dimer and monomer. (A) Sub A and (B) Sub B in the dimer. It was identified that the observed fluorescence lifetime of the dimer, τ_1^{obs} = 0.848 ps, is from Sub B and τ_2^{obs} = 4.77 ps is from Sub A. Inserts denote six fastest ET donors both in Sub A and Sub B. The distribution in the monomer is also shown in (C) Monomer. The data are taken from [56]. (Reproduced by permission of The Royal Society of Chemistry).

respectively), while in the dimer, they are Tyr55 and Tyr228 (0.95 and 0.96 nm) in Sub A and Tyr228 and Tyr314 (0.99 and 1.02 nm) in Sub B. The donor-acceptor Rc distances in the DAOB monomer are, therefore, modified substantially upon formation of the dimer. The H-bond distances between Iso and the nearby amino acids in DAOB are shown in **Table 3**. In the DAOB monomer, IsoN3H forms H-bonds with Leu51, IsoN5 with Ala49, IsoO4 with Leu51, and IsoO2 with Gly315 and Thr317 (see **Chart 1** for the atomic notations). In the dimer, Iso forms H-bonds with Leu51, Asp 49, and Thr317 in Sub A and only with Leu51 and Ala49 in Sub B. The H-bonds of IsoO4 with Leu51 and Gly50 dissociate in the dimer, and in addition the H-bond of IsoO2 with Thr317 dissociates in Sub B as does the H-bond of BzO1 (one of two carboxylate O atoms in Bz) with Tyr228OH. Thus, H-bond structures between Iso or Bz and the nearby amino acids are greatly modified upon dimer formation.

Figure 6 shows comparison of distributions of ln Rate from aromatic amino acids and Bz to Iso* among DAOB monomer and Sub A and Sub B in DAOB dimer [55, 56]. The distribution of Bz in the DAOB monomer shifts to smaller values compared to those of DAOB dimer.

9. Nonequivalent structure between the two subunits in the DAOB dimer in solution

The MDS structures of DAOB dimer and monomer are shown in **Figure 7** [56]. The local structures near Iso display quietly different between the two subunits. The H-bond pairs and

http://dx.doi.org/10.5772/intechopen.68645

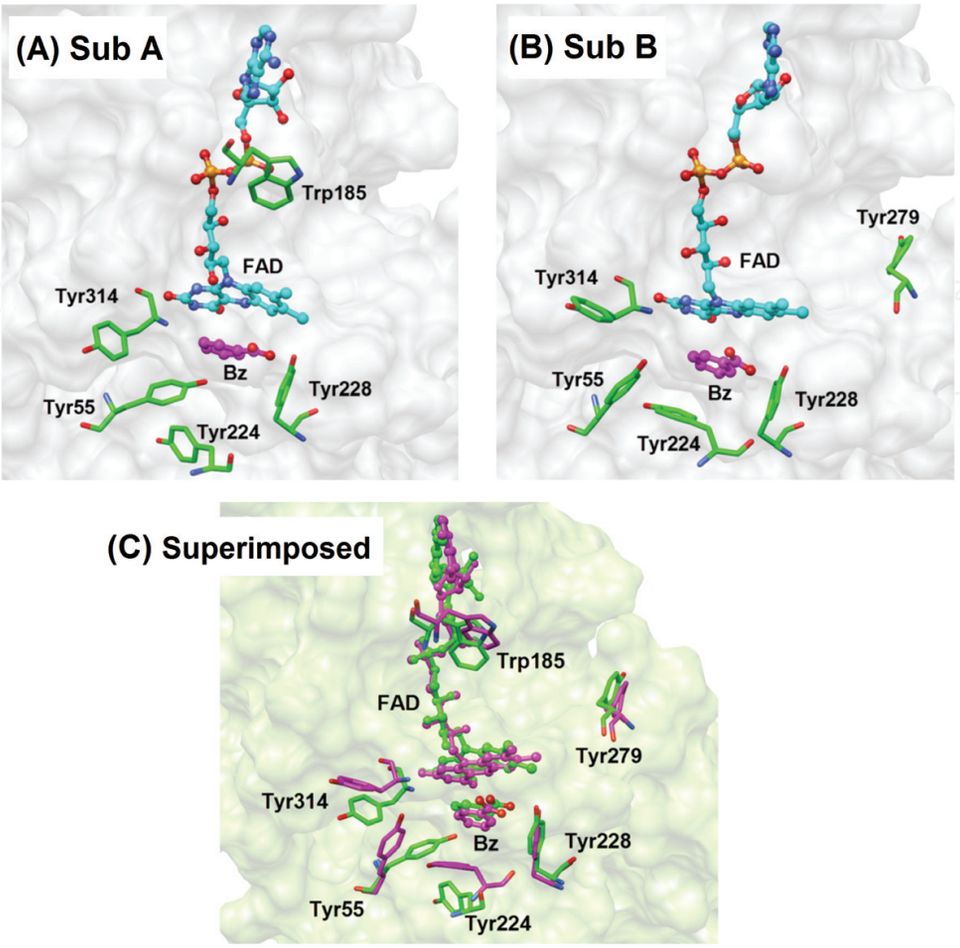

Figure 7. Structure of DAOB dimer at FAD binding site. (A) Sub A, (B) Sub B show subunits A and B in DAOB dimer. (C) Superimposed shows superimposition of Sub A and Sub B. The potential ET donors, Bz, Tyr224, Tyr228, Tyr314, Tyr55, Tyr279, and Trp185, are shown in addition to FAD. In bottom panel FAD and the aromatic amino acids are indicated in green for Sub A, and in magenta for Sub B. MDS calculation was performed at 20 °C. The data are taken from [56]. (Reproduced by permission of the Royal Society of Chemistry).

distances in DAOB also differ between them (see **Table 3**), where the H-bonds between IsoO2 and Thr317 and between BzO1 and Tyr228 in Sub A dissociate in Sub B.

Figure 8 shows ultrafast fluorescence dynamics of DAOB dimer [23]. It is evident that the dimer displayed two lifetime components at any wavelengths monitored. **Table 7** lists the decay parameters at several wavelengths. The mean lifetimes are listed in **Table 6**, 0.848 and 4.77 ps, of which fluorescence is from Sub B and Sub A, respectively [56]. The three main ET donors in the DAOB dimer are Bz, Tyr228, and Tyr55 in Sub A and Bz, Tyr228, and Tyr314 in Sub B, while the three fastest are Bz, Tyr228, and Tyr224 donor in the DAOB monomer. The ET rates and NetES in the DAOB dimer and monomer are listed in **Table 5**. The ET rate from Bz is 7.50×10^{-2} ps^{-1} in Sub A and $8.92 \times 10^{-}1$ ps^{-1} in Sub B of the DAOB dimer. The ET rates from Tyr228 and Tyr55 are also quite different between Sub A and Sub B in the DAOB dimer. Thus, the NetES values are not equivalent in the main donors between Sub A and Sub B.

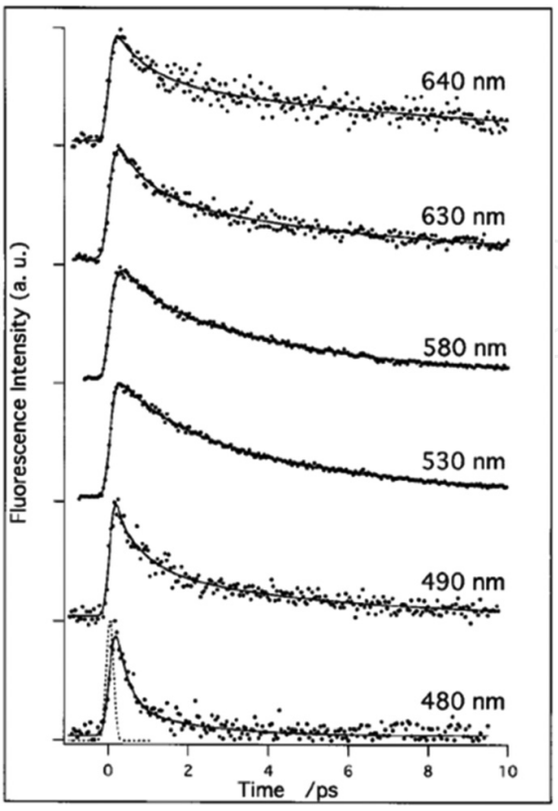

Figure 8. Fluorescence dynamics of DAOB dimer observed at various emission wavelengths. The instrumental response (fwhm ~210 fs) is also indicated with dotted line at the bottom. The decay parameters are listed in **Table 6**. (Reprinted with permission from [23]. Copyright (2000) American Chemical Society).

Wavelength (nm)	a_1	a_2	τ_1 (fs)	τ_2 (ps)	χ^2
480	0.815	0.185	300	1.90	0.74
485	0.710	0.290	420	4.23	0.62
490	0.600	0.400	506	4.46	0.64
510	0.220	0.780	942	4.47	0.10
530	0.337	0.663	1486	4.95	0.04
550	0.360	0.640	1460	5.00	0.05
580	0.260	0.740	940	4.52	0.06
600	0.250	0.750	877	4.40	0.17
630	0.486	0.514	840	6.46	0.35
640	0.470	0.530	713	7.34	1.05

The fluorescence decay functions are expressed by $F(t) = \alpha_1 \exp(-t/\tau_1) + \alpha_2 \exp(-t/\tau_2)$, where τ_1 and τ_2 are lifetimes of the fluorescent components 1 and 2, respectively, and α_1 and α_2 are their respective fractions. The chi-square (χ^2) value between the observed and calculated intensities with the two exponential decay functions is shown. The lifetimes are emission wavelength dependent. (Reprinted with permission from [23]. Copyright (2000) American Chemical Society).

Table 7. Fluorescence decay parameters of the DAOB dimer.

10. Comparison between DAAO and DAOB

The Sub A and Sub B structures of DAOB are almost equivalent in crystal, at least near the FAD binding sites [10]. However, the superimposed MDS-derived Sub A and Sub B structures in solution revealed that the structures near the Iso binding sites are not equivalent [56]. Further, the structures are quite different between the crystal Sub A and MDS-derived Sub A and between the crystal Sub B and MDS-derived Sub B. This may be ascribed that, in the crystal structure, the protein molecules are under the crystal field in the cell units, and so that not many water molecules, while in solution the protein can be relaxed in freely mobile water molecules.

It is evident that the structures near Iso in DAAO are markedly modified upon complex formation with Bz. Absorption spectrum of DAAO is much modified upon binding of Bz. The peak wavelength of the absorption band at around 450 nm of DAAO [39] shifts toward longer wavelength by 13 nm in the complex with vibrational structure [23]. The fluorescence lifetime of the DAOB monomer is 60 ps [45], while ca. 130 [44] or 200 ps [46] in DAAO monomer. The lifetimes of the DAOB dimer stated above [23] are much shorter compared to those of DAAO dimer and DAOB monomer. The remarkably shorter lifetimes in DAOB dimer are mainly ascribed to the ET from Bz to Iso*. To compare the conformation of the DAAO and DAOB using the Rc values of the aromatic amino acids other than Bz, the Rc values in the DAAO dimer at 20°C are taken as the average of those at 10 and 30°C. The Rc values of Tyr224 in the DAAO dimer, 0.82 nm in Sub A, and 0.76 nm in Sub B (**Table 2**) are much smaller than in Sub A (1.32 nm) and Sub B (1.04 nm) in the DAOB dimer. The values of Rc of Tyr228 in the DAAO dimer (0.84 nm in Sub A and 0.82 nm in Sub B) are smaller than in the DAOB dimer (0.96 nm in Sub A and 0.99 nm in Sub B), while those for Tyr55 in the DAAO dimer (1.27 nm in Sub A and 1.03 nm in Sub B) are larger than in Sub A (0.95 nm) but broadly similar to that in Sub B (1.05 nm) in the DAOB dimer. Thus, the Rc values are greatly modified upon the binding of Bz.

Root of mean square fluctuation (RMSF) is considered to be a useful index for protein fluctuation. **Figure 9** shows RMSF values against residue numbers in all four species. The mean RMSF values over all amino acids and FAD are the smallest in the DAOB dimer (0.191 and 0.171 in Sub A and Sub B, respectively) among the four proteins, the DAOB monomer (0.522) and DAAO (0.347, 0.344, and 0.701 in the dimer Sub A, Sub B, and the monomer, respectively). It is well known that the binding of Bz to DAAO greatly stabilizes the protein, and indeed this trait is used in the purification procedure of DAAO [78]. It is also recognized that the DAAO monomer is the most unstable among the DAAO and DAOB species, and so the mean RMSF may be related to protein stability in general. In fact the dissociation constant of FAD is the least in DAOB dimer and the greatest in DAAO monomer [42, 43, 45]. Denaturation of DAAO easily takes place after FAD dissociation.

The static dielectric constants (ε_0^{DA}) between Iso and ET donors within 1 nm from Iso are compared in both DAAO and DAOB [53–56], where the dielectric constants are larger (5.7–5.9) in the DAAO isomers than in the DAOB isomers (2.45–2.64), as shown in **Table 4**.

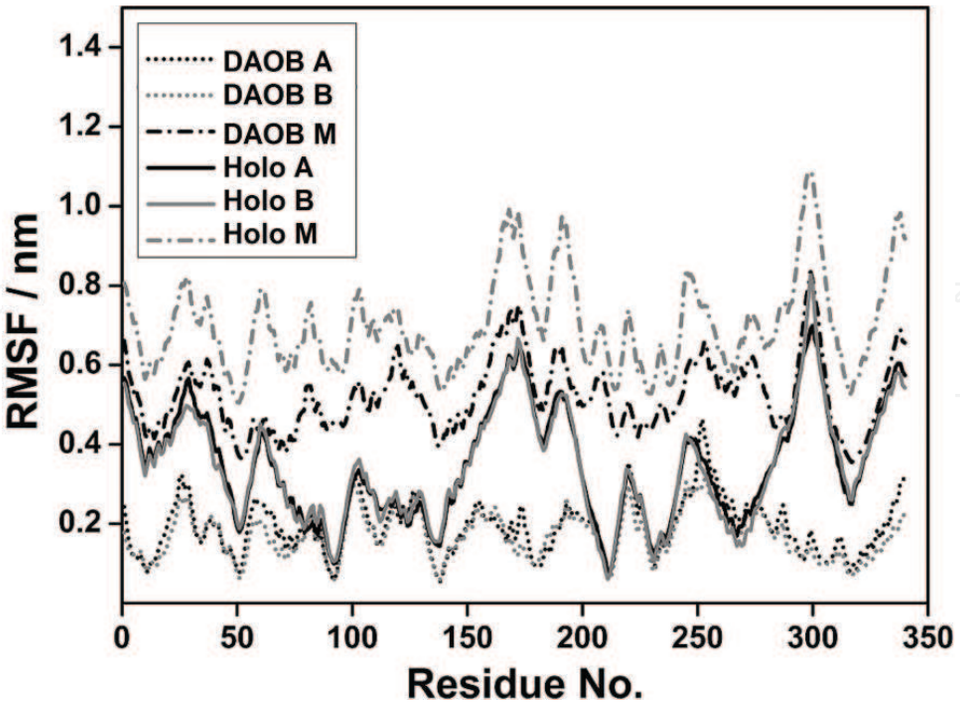

Figure 9. Comparison of root of mean square fluctuations among DAAO dimer, DAAO monomer, DAOB dimer, and DAOB monomer. Root of mean square fluctuations (RMSFs) were obtained by AMBER 10. Holo M, Holo A, and Holo B in the insert denote the DAAO monomer, Sub A, and Sub B of the DAAO dimer, respectively. DAOB M, DAOB A, and DAOB B denote the DAOB monomer, Sub A, and Sub B of the DAOB dimer, respectively. RMSFs of DAAO monomer were taken from [54], those for DAAO dimer from [53] and those of DAOB monomer from [55], and DAOB dimer from [56]. (Reproduced by permission of the Royal Society of Chemistry).

The polarity near Iso is considered to be higher when the value of ε_0^{DA} is higher. The radial distribution functions (RDFs) of water molecules and numbers of water molecules near Iso are reported in DAAO dimer [53] and in DAOB [56]. The RDFs of DAAOs are shown in **Figure 10**. At 10°C approximately 5.5 and 16 molecules are predicted to exist near Iso in Sub A and Sub B, respectively, while at 30°C this switched to 12 and 6 water molecules in Sub A and Sub B, respectively. The number of water molecules could also relate to polarity around Iso. The RDF in DAOB is shown in **Figure 11**, where in the DAOB dimers are few if any, and five water molecules existed near Iso in Sub A and Sub B, respectively. No water molecules are predicted to exist near Iso in the DAOB monomer. Thus, the number of water molecules is much greater in the DAAO dimer than that in DAOB dimer and the monomer, which is in accordance with the ε_0^{DA} results. Stokes shift of the fluorescence spectra in flavoproteins is related to the polarity around Iso. The fluorescence spectra of Iso display at 523 nm of peak wavelength in the DAOB dimer [23] and at 530 nm in DAAO [39]. The ε_0^{DA} values obtained by ET analyses and the RDF of water molecules obtained by MDS are both in accordance with the behavior of the fluorescence spectra.

http://dx.doi.org/10.5772/intechopen.68645

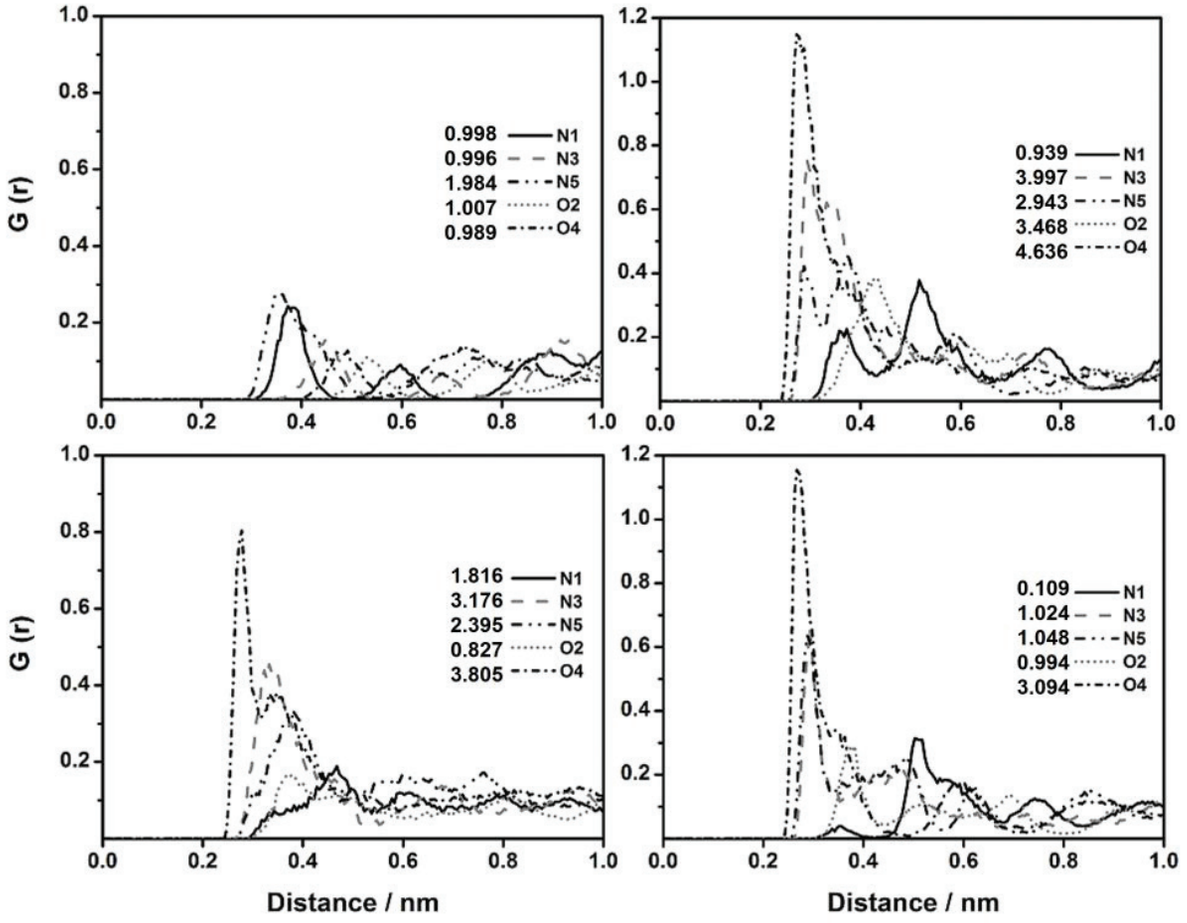

Figure 10. (A) Sub A 10 °C, (B) Sub B 10 °C, (C) Sub A 30 °C and (D) Sub B 30 °C show the radial distribution function derived number of water molecules near hetero atoms in Iso ring in the DAAO dimer. The vertical axes, G(r), denote the radial distribution function. Inserts indicate mean numbers of water molecules at the distances of first layer from the hetero atoms in Iso (see **Chart 1** for atom notations). The data are taken from [53]. Reproduced by permission of the PCCP Owner Societies.

11. Conclusions

MDS is a useful tool to study the structures of DAAO and DAOB in solution, while their experimental fluorescence lifetimes are also a useful index to monitor their structural changes, because the fluorescence lifetimes in flavoproteins are determined by the rates of ET from the aromatic amino acids to Iso*. Thus, combining the MDS structures and the experimental fluorescence lifetimes by ET analysis provides more precise information on the submicroscopic features of the structures of DAAO and DAOB. It is concluded as follows:

1. The origin of the cooperativity in the FAD binding processes is due to much lower (1/74 fold) dissociation constant of FAD in the DAAO dimer than in the monomer. The structural

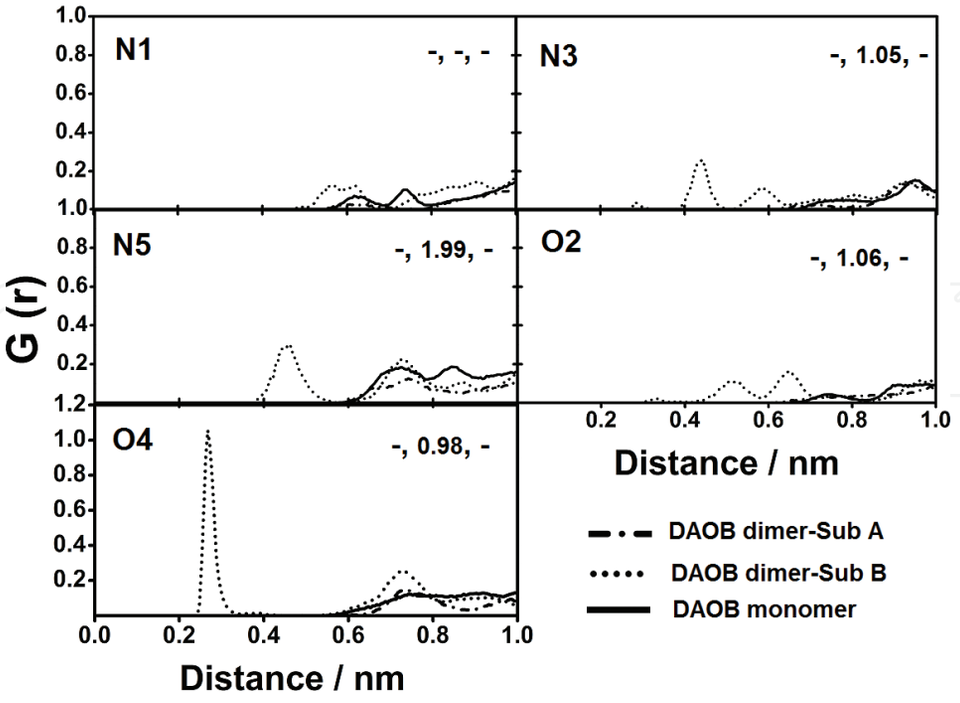

Figure 11. Radial distribution function of water molecules near the heteroatoms of Iso in DAOB. Vertical axes, G(r), denote the radial distribution functions. Red, blue, and black numbers showed the mean number of water molecules in Sub A and Sub B of DAOB dimer, and DAOB monomer is indicated in red, blue, and black, respectively. The data for the DAOB dimer are taken from [56] and for DAOB monomer from [55]. (Reproduced by permission of The Royal Society of Chemistry).

basis for the cooperative binding in DAAO is elucidated by differences in the H-bond structures, the Rc, and the NetES values between the DAAO dimer and the monomer.

2. The temperature-induced transition in the DAAO monomer is ascribed to the differences in the SFEG and NetES between the two temperatures. The change in the SFEG with temperature may be brought about by the change in H-bond structures.

3. The two subunits of the DAAO dimer are not equivalent in solution, as revealed by MDS and ET analyses.

4. The structures of DAOB dimer are almost equivalent for the two subunits in the crystal but are nonequivalent in solution as revealed by the experimental fluorescence lifetimes, MDS structures, and ET analyses.

5. The mean RMSF values over all residues are the smallest in the DAOB dimer and the largest in the DAAO monomer. It is well recognized that the binding of Bz to DAAO greatly stabilizes the protein and the DAAO monomer is the most unstable among the DAAO and DAOB isomers. The mean RMSF may be related to protein stability in general.

6. The ε_0^{DA} values in the DAAO isomers (5.7–5.9) are much larger than those in the DAOB isomers (2.45–2.64), which are elucidated by the number of water molecules near Iso, as derived from the RDF analysis. Water molecules in DAAO are excluded upon the binding of competitive inhibitor of Bz.

7. The Stokes shift of the fluorescence spectra is related to the polarity around Iso, with a change in the emission peak from 524 nm in the DAOB dimer to 530 nm in the DAAO dimer. The ε_0^{DA} values obtained by ET analysis and number of water molecules near Iso obtained by RDF analyses are both in accordance with the observed Stokes shift.

Acknowledgements

A. N. would like to acknowledge the postdoctoral fellowship of Chulalongkorn University. F.T. is thankful for financial support from the Ratchadaphiseksomphot Endowment Fund and a short-term visit grant from Chulalongkorn University. We would like to thank the Computational Chemistry Unit Cell, Chulalongkorn University and The National e-Science Infrastructure Consortium for providing computing resources. S. T. thankful for the Japan Society for the Promotion of Science (Grants-in-Aid for Scientific Research No. 26410029).

Author details

Arthit Nueangaudom[1], Kiattisak Lugsanangarm[2], Somsak Pianwanit[1], Sirirat Kokpol[1], Nadtanet Nunthaboot[3], Fumio Tanaka[1,4]*, Seiji Taniguchi[4]* and Haik Chosrowjan[4]

*Address all correspondence to: fumio.tanaka@yahoo.com and taniguchi@ilt.or.jp

1 Department of Chemistry, Faculty of Science, Chulalongkorn University, Bangkok, Thailand

2 Program of Chemistry, Faculty of Science and Technology, Bansomdejchaopraya Rajabhat University, Bangkok, Thailand

3 Department of Chemistry and Center of Excellence for Innovation in Chemistry, Faculty of Science, Mahasarakham University, Mahasarakham, Thailand

4 Division of Laser Biochemistry, Institute for Laser Technology, Osaka, Japan

References

[1] Horiike K, Ishida T, Tanaka H, Arai R. Distribution of D-amino acid oxidase and D-serine in vertebrate brains. Journal of Molecular Catalysis B: Enzymatic 2001;**12**:37–41

[2] Miura R, Setoyama C, Nishina Y, Shiga K, Miyahara I, Mizutani H, Hirotsu K. Porcine kidney d-amino acid oxidase: The three-dimensional structure and its catalytic mechanism based on the enzyme–substrate complex model. Journal of Molecular Catalysis B: Enzymatic 2001;**12**:43-52

[3] Tishkov VI, Khoronenkova SV. d-Amino acid oxidase: Structure, catalytic mechanism, and practical application. Biochemistry (Moscow). 2005;**70**:40-54

[4] Pollegioni L, Piubelli L, Sacchi S, Pilone MS, Molla G. Physiological functions of d-amino acid oxidases: From yeast to humans. Cellular and Molecular Life Sciences 2007;**64**:1373-1394

[5] Kawazoe T, Park HK, Iwana S, Tsuge H, Fukui K. Human d-amino acid oxidase: An update and review. Chemical Record 2007;**7**:305-315

[6] Sacchi S, Caldinelli L, Cappelletti P, Pollegioni L, Molla G. Structure–function relationships in human d-amino acid oxidase. Amino Acids 2012;**43**:1833-1850

[7] Madeira C, Freitas ME, Vargas-Lopes C, Wolosker H, Panizzutti R. Increased brain d-amino acid oxidase (DAAO) activity in schizophrenia. Schizophrenia Research. 2008;**101**:76-83

[8] Boks MPM, Rietkerk T, van de Beek MH, Sommer IE, de Koning TJ, Kahn RS. Reviewing the role of the genes G72 and DAAO in glutamate neurotransmission in schizophrenia. European Neuropsychopharmacology 2007;**17**:567-572

[9] Katane M, Osaka N, Matsuda S, Maeda K, Kawata T, Saitoh Y, Sekine M, Furuchi T, Doi I, Hirono S, Homma H: Identification of novel d-amino acid oxidase inhibitors by in silico screening and their functional characterization in vitro. Journal of Medicinal Chemistry 2013;**56**:1894-1907

[10] Mizutani H, Miyahara I, Hirotsu K, Nishina Y, Shiga K, Setoyama C, Miura R. Three-dimensional structure of porcine kidney d-amino acid oxidase at 3.0 Å resolution. Journal of Biochemistry. 1996;**120**:14-17

[11] Mattevi A, Vanoni MA, Todone F, Rizzi M, Teplyakov A, Coda A, Bolognesi M, Curti B. Crystal structure of d-amino acid oxidase: a case of active site mirror-image convergent evolution with flavocytochrome b2. Proceedings of the National Academy of Sciences of the United States of America. 1996;**93**:7496-7501

[12] Weber G. Fluorescence of riboflavin, diaphorase and related substances [thesis]. Cambridge: University of Cambridge; 1947

[13] Weber G. The quenching of fluorescence in liquids by complex formation. Determination of the mean life of the complex. Transactions of the Faraday Society. 1948;**44**:185-189

[14] Weber G. Fluorescence of riboflavin and flavin-adenine dinucleotide. Biochemical Journal 1950;**47**:114-121

[15] Spencer RD, Weber G. Structure and Function of Oxidation-Reduction Enzymes. In: Åkeson Å, Ehrenberg A, editors. Oxford: Pergamin Press; 1972. p. 393-399.

[16] Weber G, Tanaka F, Okamoto BY, Drickamer HG. The effect of pressure on the molecular complex of isoalloxazine and adenine. Proceedings of the National Academy of Sciences of the United States of America. 1974;**71**:1264-1266

[17] McCormick DB. Interactions of flavins with amino acid residues: Assessments from spectral and photochemical studies. Photochemistry and Photobiology 1977;**26**:169-182

[18] van den Berg PA, Visser AJWG. In: Valeur B, Brochon JC, editors. Tracking molecular dynamics of flavoproteins with time-resolved fluorescence spectroscopy. Berlin: Springer; 2001. p. 457-485

[19] Karen A, Ikeda N, Mataga N, Tanaka F. Picosecond laser photolysis studies of fluorescence quenching mechanisms of flavin: a direct observation of indole-flavin singlet charge transfer state formation in solutions and flavoenzymes. Photochemistry and Photobiology 1983;**37**:495-502

[20] Karen A, Sawada MT, Tanaka F, Mataga N. Dynamics of excited flavoproteins-picosecond laser photolysis studies. Photochemistry and Photobiology 1987;**45**:49-53

[21] Zhong D, Zewail AH. Femtosecond dynamics of flavoproteins: Charge separation and recombination in riboflavine (vitamin B2)-binding protein and in glucose oxidase enzyme. Proceedings of the National Academy of Sciences of the United States of America. 2001;**98**:11867-11872

[22] Mataga N, Chosrowjan H, Shibata Y, Tanaka F. Ultrafast fluorescence quenching dynamics of flavin chromophores in protein nanospace. Journal of Physical Chemistry B 1998;**102**:7081-7084

[23] Mataga N, Chosrowjan H, Shibata Y, Tanaka F, Nishina Y, Shiga K. Dynamics and mechanisms of ultrafast fluorescence quenching reactions of flavin chromophores in protein nanospace. Journal of Physical Chemistry B 2000;**104**:10667-10677

[24] Mataga N, Chosrowjan H, Taniguchi S, Tanaka F, Kido N, Kitamura M. Femtosecond fluorescence dynamics of flavoproteins:comparative studies on flavodoxin, its site-directed mutants, and riboflavin binding protein regarding ultrafast electron transfer in protein nanospaces. Journal of Physical Chemistry B 2002;**106**:8917-8920

[25] Tanaka F, Chosrowjan H, Taniguchi S, Mataga N, Sato K, Nishina Y, Shiga K. Donor-acceptor distance-dependence of photoinduced electron-transfer rate in flavoproteins. Journal of Physical Chemistry B 2007;**111**:5694-5699

[26] Chosrowjan H, Taniguchi S, Mataga N, Tanaka F, Todoroki D, Kitamura M. Comparison between ultrafast fluorescence dynamics of FMN binding protein from desulfovibrio vulgaris, strain miyazaki, in solution vs crystal phases. Journal of Physical Chemistry B 2007;**111**:8695-8697

[27] Chosrowjan H, Taniguchi S, Mataga N, Tanaka F, Todoroki D, Kitamura M. Ultrafast fluorescence dynamics of FMN-binding protein from Desulfovibrio vulgaris (Miyazaki F) and its site-directed mutated proteins. Chemical Physics Letters 2008;**462**:121-124

[28] Chosrowjan H, Taniguchi S, Mataga N, Nakanishi T, Haruyama Y, Sato S, Kitamura M, Tanaka F. Effects of the disappearance of one charge on ultrafast fluorescence dynamics of the FMN binding protein. Journal of Physical Chemistry B 2010;**114**:6175-6182

[29] Chosrowjan H, Taniguchi S, Wongnate T, Sucharitakul J, Chaiyen P, Tanaka F. Conformational heterogeneity in pyranose 2-oxidase from Trametes multicolor revealed by ultrafast fluorescence dynamics. Journal of Photochemistry and Photobiology A 2012;**234**:44-48

[30] Taniguchi S, Chosrowjan H, Wongnate T, Sucharitakul J, Chaiyen P, Tanaka F. Ultrafast fluorescence dynamics of flavin adenine dinucleotide in pyranose 2-oxidases variants and their complexes with acetate: Conformational heterogeneity with different dielectric constants. Journal of Photochemistry and Photobiology A 2012;**245**:33-42

[31] Nunthaboot N, Tanaka F, Kokpol S, Chosrowjan H, Taniguchi S, Mataga N. Simultaneous analysis of ultrafast fluorescence decays of FMN binding protein and its mutated proteins by molecular dynamic simulation and electron transfer theory. Journal of Physical Chemistry B 2008;**112**:13121-13127

[32] Nunthaboot N, Pianwanit S, Kokpol S, Tanaka F. Simultaneous analyses of photoinduced electron transfer in the wild type and four single substitution isomers of the FMN binding protein from Desulfovibrio vulgaris, Miyazaki F. Physical Chemistry Chemical Physics 2011;**13**:6085-6097

[33] Nunthaboot N, Kido N, Tanaka F, Lugsanangarm K, Nueangaudom A, Pianwanit S, Kokpol S. Relationship between rate of photoinduced electron transfer and hydrogen bonding chain of tyrosine-glutamine-flavin in flavin photoreceptors: Global analyses among four TePixDs and three AppAs. Journal of Photochemistry and Photobiology A 2013;**252**:14-24

[34] Lugsanangarm K, Pianwanit S, Kokpol S, Tanaka F, Chosrowjan H, Taniguchi S, Mataga N. Analysis of photoinduced electron transfer in flavodoxin. Journal of Photochemistry and Photobiology A 2011;**217**:333-340

[35] Lugsanangarm K, Pianwanit S, Kokpol S, Tanaka F, Chosrowjan H, Taniguchi S, Mataga N. Photoinduced electron transfer in wild type and mutated flavodoxin from Desulfovibrio vulgaris, strain Miyazaki F.: Energy gap law. Journal of Photochemistry and Photobiology A. 2011;**219**:32-41.

[36] Lugsanangarm K, Pianwanit S, Nueangaudom A, Kokpol S, Tanaka F, Nunthaboot N, Ogino K, Takagi R, Nakanishi T, Kitamura M, Taniguchi S, Chosrowjan H. Mechanism of photoinduced electron transfer from tyrosine to the excited flavin in the flavodoxin from Helicobacter pylori. A comparative study with the flavodoxin and flavin mononucleotide binding protein from Desulfovibrio vulgaris (Miyazaki F). Journal of Photochemistry and Photobiology A 2013;**268**:58-66

[37] Kozioł J. Studies on flavins in organic solvents - III. Spectral behaviour of lumiflavin. Photochemistry and Photobiology. 1969;**9**:45-53

[38] Kotaki A, Yagi K. Fluorescence properties of flavins in various solvents. The Journal of Biochemistry (Tokyo). 1970;**68**:509-516

[39] Massey V, Curti B, Ganther H. A temperature-dependent conformational change in D-amino acid oxidase and its effect on catalysis. Journal of Biological Chemistry 1966;**241**:2347-2357

[40] Wu FY-H, Tu S-C, Wu C-W, McCormick DB. Characteristics of the fluorescence spectra of apoenzyme and flavin portions of D-amino acid oxidase. Biochemical and Biophysical Research Communications 1970;**41**:381-385

[41] Yagi K, Tanaka F, Ohishi N. Structure and function of D-amino acid oxidase IX. Changes in the fluorescence polarization of FAD upon complex formation. Journal of Biochemistry (Tokyo). 1975;**77**:463-468

[42] Tanaka F, Yagi K. Cooperative binding of coenzyme in D-amino acid oxidase. Biochemistry 1979;**18**:1531-1536

[43] Tanaka F, Yagi K. Cooperative binding of flavin adenine dinucleotide accompanied by the change in the quaternary structure of D-amino acid oxidase. In: Yagi K, Yamano T, editors. Flavins and Flavoproteins. Tokyo, Japan: Japan Scientific Press; 1980. p. 1091-1094

[44] Nakashima N, Yoshihara K, Tanaka F, Yagi K. Picosecond fluorescence lifetime of the coenzyme of D-amino acid oxidase. Journal of Biological Chemistry 1980;**255**:5261-5263

[45] Yagi K, Tanaka F, Nakashima N, Yoshihara K. Picosecond laser fluorometry of FAD of D-amino acid oxidase-benzoate complex. Journal of Biological Chemistry 1983;**258**:3799-3802

[46] Tanaka F, Tamai N, Yamazaki I, Nakashima N, Yoshihara K. Temperature-induced changes in the coenzyme environment of D-amino acid oxidase revealed by the multiple decays of FAD fluorescence. Biophysical Journal 1989;**56**:901-909

[47] Tanaka F, Tamai N, Yamazaki I. Picosecond-resolved fluorescence spectra of D-amino acid oxidase. A new fluorescent species of the coenzyme. Biochemistry 1989;**28**:4259-4262

[48] Case DA, Darden TA, Cheatham ITE, Simmerling CL, Wang J, Duke RE, Luo R, Crowley M, Walker RC, Zhang W, Merz KM, Wang B, Hayik S, Roitberg A, Seabra G, Kolossváry I, Wong KF, Paesani F, Vanicek J, Wu X, Brozell SR, Steinbrecher T, Gohlke H, Yang L, Tan C, Mongan J, Hornak V, Cui G, Mathews DH, Seetin MG, Sagui C, Babin V, Kollman PA. AMBER 10. San Francisco: University of California; 2008.

[49] Wang J, Cieplak P, Kollman PA. How well does a restrained electrostatic potential (RESP) model perform in calculating conformational energies of organic and biological molecules? Journal of Computational Chemistry 2000;**21**:1049-1074

[50] Bayly CI, Cieplak P, Cornell W, Kollman PA. A well-behaved electrostatic potential based method using charge restraints for deriving atomic charges: The RESP model. Journal of Physical Chemistry 1993;**97**:10269-10280

[51] Essmann U, Perera L, Berkowitz ML, Darden T, Lee H, Pedersen LG. A smooth particle mesh Ewald method. Journal of Chemical Physics 1995;**103**:8577-8593

[52] Ryckaert J-P, Ciccotti G, Berendsen HJC. Numerical integration of the cartesian equations of motion of a system with constraints: Molecular dynamics of n-alkanes. Journal of Computational Physics 1977;**23**:327-341

[53] Nueangaudom A, Lugsanangarm K, Pianwanit S, Kokpol S, Nunthaboot N, Tanaka F. Non-equivalent conformations of D-amino acid oxidase dimer from porcine kidney between the two subunits. Molecular dynamics simulation and photoinduced electron transfer. Physical Chemistry Chemical Physics 2014;**16**:1930-1944

[54] Nueangaudom A, Lugsanangarm K, Pianwanit S, Kokpol S, Nunthaboot N, Tanaka F. Structural basis for the temperature-induced transition of D-amino acid oxidase from pig kidney revealed by molecular dynamic simulation and photo-induced electron transfer. Physical Chemistry Chemical Physics 2012;**14**:2567-2578

[55] Nueangaudom A, Lugsanangarm K, Pianwanit S, Kokpol S, Nunthaboot N, Tanaka F. The mechanism of photoinduced electron transfer in the D-amino acid oxidase–benzoate complex from pig kidney: Electron transfer in the inverted region. Journal of Photochemistry and Photobiology A 2012;**250**:6-17

[56] Nueangaudom A, Lugsanangarm K, Pianwanit S, Kokpol S, Nunthaboot N, Tanaka F, Taniguchi S, Chosrowjan H. Theoretical analyses of the fluorescence lifetimes of the D-amino acid oxidase-benzoate complex dimer from porcine kidney: Molecular dynamics simulation and photoinduced electron transfer. RSC Advances 2014;**4**:54096-54108

[57] Marcus RA. On the theory of oxidation-reduction reactions involving electron transfer I. Journal of Chemical Physics 1956;**24**:966-978

[58] Marcus RA. Electrostatic free energy and other properties of states having nonequilibrium polarization I. Journal of Chemical Physics 1956;**24**:979-989

[59] Marcus RA. Chemical and electrochemical electron-transfer theory. Annual Review of Physical Chemistry 1964;**15**:155-196

[60] Hush NS. Adiabatic theory of outer sphere electron-transfer reactions in solution. Transactions of the Faraday Society 1961;**57**:557-580

[61] Warshel A, Chu Z, Parson W. Dispersed polar on simulations of electron transfer in photosynthetic reaction centers. Science 1989;**246**:112-116

[62] Warshel A, Parson W. Computer simulations of electron-transfer reactions in solution and in photosynthetic reaction centers. Annual Review of Physical Chemistry 1991;**42**:279-309

[63] Bixon M, Jortner J. Non-Arrhenius temperature dependence of electron-transfer rates. Journal of Physical Chemistry 1991;**95**:1941-1944

[64] Bixon M, Jortner J. Charge separation and recombination in isolated supermolecules. Journal of Physical Chemistry 1993;**97**:13061-13066

[65] Bixon M, Jortner J, Cortes J, Heitele H, Michel-Beyerle ME. Energy gap law for nonradiative and radiative charge transfer in isolated and in solvated supermolecules. Journal of Physical Chemistry 1994;**98**:7289-7299

[66] Kakitani T, Mataga N. New energy gap laws for the charge separation process in the fluorescence quenching reaction and the charge recombination process of ion pairs produced in polar solvents. Journal of Physical Chemistry 1985;**89**:8-10

[67] Kakitani T, Yoshimori A, Mataga N. Effects of the donor-acceptor distance distribution on the energy gap laws of charge separation and charge recombination reactions in polar solutions. Journal of Physical Chemistry 1992;**96**:5385-5392

[68] Matsuda N, Kakitani T, Denda T, Mataga N. Examination of the viability of the Collins-Kimball model and numerical calculation of the time-dependent energy gap law of photoinduced charge separation in polar solution. Chemical Physics 1995;**190**:83-95

[69] Moser CC, Keske JM, Warncke K, Farid RS, Dutton PL. Nature of biological electron transfer. Nature 1992;**355**:796-802

[70] Beratan D, Betts J, Onuchic J. Protein electron transfer rates set by the bridging secondary and tertiary structure. Science 1991;**252**:1285-1288

[71] Bendall DS. Protein Electron Transfer. Oxford: BIOS Scientific; 1996

[72] Gray HB, Winkler JR. Electron transfer in proteins. Annual Review of Biochemistry 1996;**65**:537-561

[73] Warshel A, Parson W. Dynamics of biochemical and biophysical reactions: Insight from computer simulations. Quarterly Reviews of Biophysics. 2001;**34**:563-679

[74] Vorsa V, Kono T, Willey KF, Winograd N. Femtosecond photoionization of ion beam desorbed aliphatic and aromatic amino acids:Fragmentation via α-cleavage reactions. Journal of Physical Chemistry B 1999;**103**:7889-7895

[75] Fonda ML, Anderson BM. D-amino acid oxidase : III. Studies of flavin adenine dinucleotide binding. Journal of Biological Chemistry. 1968;**243**:5635-5643

[76] Henn SW, Ackers GK. Molecular sieve studies of interacting protein systems. V. Association of subunits of D-amino acid oxidase apoenzyme. Biochemistry. 1969;**8**:3829-3838

[77] Henn SW, Ackers GK. Molecular sieve studies of interacting protein systems: IV. Molecular size of the D-amino acid oxidase apoenzyme subunit. Journal of Biological Chemistry. 1969;**244**:465-470

[78] Yagi K, Naoi M, Harada M, Okamura K, Hidaka H, Ozawa T, Kotaki A. Structure and function of d-amino acid oxidase I. Further purification of hog kidney D-amino acid oxidase and its hydrodynamic and optical rotatory properties. Journal of Biochemistry (Tokyo). 1967;**61**:580-597

[79] Yagi K, Ohishi N. Structure and function of D-amino acid oxidase IV. Electrophoretic and ultracentrifugal approach to the monomer-dimer equilibrium. Journal of Biochemistry (Tokyo). 1972;**71**:993-998

[80] Antonini E, Brunori M, Bruzzesi MR, Chiancone E, Massey V. Association-dissociation phenomena of D-amino acid oxidase. Journal of Biological Chemistry 1966;**241**:2358-2366

[81] Tojo H, Horiike K, Shiga K, Nishina Y, Watari H, Yamano T. Self-association mode of a flavoenzyme D-amino acid oxidase from hog kidney. I. Analysis of apparent weight-average molecular weight data for the apoenzyme in terms of models. Journal of Biological Chemistry. 1985;**260**:12607-12614

[82] Tojo H, Horiike K, Shiga K, Nishina Y, Watari H, Yamano T. Self-association mode of a flavoenzyme D-amino acid oxidase from hog kidney. II. Stoichiometry of holoenzyme

association and energetics of subunit association. Journal of Biological Chemistry. 1985;**260**:12615-12621

[83] Monod J, Wyman J, Changeux J-P. On the nature of allosteric transitions: A plausible model. Journal of Molecular Biology 1965;**12**:88-118

[84] Koshland DE, Némethy G, Filmer D. Comparison of experimental binding data and theoretical models in proteins containing subunits. Biochemistry 1966;**5**:365-385

[85] Nichol LW, Jackson WJH, Winzor DJ. A theoretical study of the binding of small molecules to a polymerizing protein system. A model for allosteric effects. Biochemistry. 1967;**6**:2449-2456

[86] Nichol LW, Winzor DJ. Ligand-induced polymerization. Biochemistry 1976;**15**:3015-3019

[87] Selwood T, Jaffe EK. Dynamic dissociating homo-oligomers and the control of protein function. Archives of Biochemistry and Biophysics 2012;**519**:131-143

[88] Shiga K, Shiga T. The kinetic features of monomers and dimers in high- and low-temperature conformational states of D-amino acid oxidase. Biochimica et Biophysica Acta 1972;**263**:294-303

[89] Koster JF, Veeger C. The relation between temperature-inducible allosteric effects and the activation energies of amino-acid oxidases. Biochimica et Biophysica Acta 1968;**167**:48-63

[90] Sturtevant JM, Mateo PL. Proposed temperature-dependent conformational transition in D-amino acid oxidase: A differential scanning microcalorimetric study. Proceedings of the National Academy of Sciences of the United States of America. 1978;**75**:2584-2587